Zebrafish as a model to study PERK function in developmental diseases: implications for Wolcott-Rallison syndrome

Liliana M. Almeida[a,b], Leonor Pereira Lima [a,b], Nuno A. S. Oliveira [a,b], Rui F. O. Silva [a,b], Bruno Sousa [a,b], José Bessa [c,d], Brígida R. Pinho [a,b], Jorge M. A. Oliveira [a,b,*]

[a]UCIBIO, Applied Molecular Biosciences Unit, Mitochondria and Neurobiology Lab, Faculdade de Farmácia, Universidade do Porto, 4050-313 Porto, Portugal

[b]i4HB, Institute for Health and Bioeconomy, Universidade do Porto, 4050-313 Porto, Portugal

[c]IBMC, Instituto de Biologia Molecular e Celular, Universidade do Porto, 4200-135 Porto, Portugal

[d]i3S, Instituto de Investigação e Inovação em Saúde, Universidade do Porto, 4200-135 Porto, Portugal

***Corresponding author:**
Jorge M. A. Oliveira (jorgemao@ff.up.pt)
Departamento de Ciências do Medicamento, Laboratório de Farmacologia, Faculdade de Farmácia, Universidade do Porto
Rua de Jorge Viterbo Ferreira, 228, 4050-313 Porto, Portugal | Tel. +351 220428610

Abbreviations:
2-NBDglucose, (2-(7-Nitro-2,1,3-benzoxadiazol-4-yl)-D-glucosamine); ATF4, Activating Transcription Factor 4; CHOP, C/EBP homologous protein; dpf, days post-fertilization; dTC, d-tubocurarine; eIF2α, eukaryotic translation initiation factor 2α; ER, Endoplasmic reticulum; hfp, hours post-fertilization; GSK, GSK2606414; ISR, Integrated Stress Response; NPH, Nikon-Prior-Hamamatsu; PERK, Protein kinase R-like ER kinase; WRS, Wolcott-Rallison Syndrome

Complete text word count: 5 356

Acknowledgments: Fundação para a Ciência e a Tecnologia (FCT): UIDB/04378/2020; UIDP/04378/2020; LA/P/0140/2020; SFRH/BD/138451/2018; DL57/2016/CP1346/CT0016; PTDC/BIA-MOL/3834/2021; CEECIND/03482/2018.

Running Title: Zebrafish PERK in developmental diseases

Abstract

PERK (EIF2AK3) is an endoplasmic reticulum stress kinase whose loss of function disturbs normal human development, leading to skeletal dysplasia and permanent neonatal diabetes, as seen in the Wolcott-Rallison Syndrome (WRS). The lack of efficient and less invasive therapies for developmental diseases highlights the need for animal models that replicate the complex pathological phenotypes, while preserving scalability for drug screening. Zebrafish exhibits high fecundity and rapid development that facilitate efficient and scalable *in vivo* drug testing. Here, we aimed to assess the potential of zebrafish to study PERK function and its pharmacological modulation, and as model organism of developmental diseases such as the WRS. Using bioinformatic analyses, we showed high similarity between human and zebrafish PERK. We used the pharmacological PERK inhibitor GSK2606414, which was bioactive in zebrafish, to modulate PERK function. Using transgenic zebrafish expressing fluorescent pancreatic markers and a fluorescent glucose probe, we observed that PERK inhibition decreased β cell mass and disrupted glucose homeostasis. By combining behavioural and functional assays, we show that PERK-inhibited zebrafish present marked defects in growth and skeletal development, as well as neuromuscular and cardiac deficiencies, which are clinically relevant in WRS patients, while sparing parameters like otolith area and eye/body ratio which are not associated with WRS. These results show that zebrafish holds potential to study PERK function and its pharmacological modulation in developmental disorders like WRS, assisting research on their pathophysiology and experimental treatments.

Keywords: developmental diseases; metabolic diseases; model organism; zebrafish; PERK; Wolcott-Rallison syndrome

60 **1. Introduction**

61 Protein kinase RNA-like endoplasmic reticulum kinase (PERK) is an endoplasmic reticulum
62 (ER) membrane kinase that activates in response to disruptions in ER protein homeostasis
63 (proteostasis) by promoting a protective response, the integrated stress response (ISR). Upon
64 activation by stress, PERK phosphorylates eukaryotic translation initiation factor 2α (eIF2α)
65 that decreases global protein synthesis, alleviating nascent protein load [1] and boosts the
66 synthesis of transcription factors like activating transcription factor 4 (ATF4) and C/EBP
67 homologous protein (CHOP). These transcription factors regulate the expression of
68 chaperones, proteases and components of the autophagic pathway, thus contributing to
69 proteostasis maintenance [1]. During development, protein synthesis plays a critical role in cell
70 division, differentiation, and the rapid growth of embryos [2], and PERK is essential for
71 detecting protein misfolding and adjusting protein synthesis to maintain proteostasis [3].

72 In humans, loss-of-function mutations in the *EIF2AK3* gene encoding for PERK cause a
73 rare (prevalence of <1/1 000 000; ORPHA:1667) autosomal recessive developmental disease
74 named Wolcott-Rallison Syndrome (WRS), with patients dying before 35 years of age [4].
75 WRS is mainly characterized by skeletal dysplasia and neonatal diabetes mellitus [5], but WRS
76 patients may also present broad symptomatology like motor neuropathy, intellectual deficit,
77 early neurodegeneration, and cardiac malformations [4]. This broad symptomatology is likely
78 due to the widespread distribution of PERK, with several loss-of-function mutations totally or
79 partially abolishing its kinase activity [4, 6]. Existing therapies for WRS patients include blood
80 glucose control with insulin pumping and transplant of liver/pancreas and kidney [7]. The
81 scarcity of non-invasive and more effective therapeutic options for WRS patients highlights
82 the need for further therapeutic investigation, which requires efficient WRS models.

83 The currently available *in vivo* models for the developmental disease WRS are rodents
84 with PERK knock-out or loss-of-function mutations in PERK that exhibit the WRS hallmarks

85 – neonatal diabetes and skeletal dysplasia [8, 9] – and the broad-spectrum phenotypes – cardiac,
86 muscle and cognitive abnormalities [10-12]. However, for large exploratory studies of new
87 therapeutics, there are efficiency advantages in using small vertebrates like zebrafish before
88 testing the most promising candidates in rodent models. Zebrafish are increasingly used to
89 develop disease models given their advantageous features: high fecundity, external
90 fertilization, and rapid formation of complete organs, making zebrafish ideal for investigating
91 developmental diseases and for rapid and scalable *in vivo* drug testing [13, 14]. Previous studies
92 that targeted PERK in zebrafish, used either genetic (morpholino knockdown) or
93 pharmacological inhibition [15-17]. In such studies, PERK inhibition with GSK2606414 was
94 used in zebrafish adults to study sleep regulation [15], and PERK inhibition with GSK2656157
95 or PERK knockdown was used to study redox regulation and neurogenesis in zebrafish
96 embryos [16, 17]. To the best of our knowledge, there are no previous studies in zebrafish with
97 a primary focus on studying PERK function in developmental diseases, including WRS.
98 Here, we combined bioinformatic analyses, molecular biology techniques, behaviour,
99 and functional assays to assess the effects of pharmacological PERK inhibition in zebrafish.
100 We used transgenic zebrafish expressing pancreatic reporters and a fluorescent glucose probe
101 to assess diabetic-like phenotypes. We performed functional and structural microscopy to
102 assess skeletal, neuromuscular, and cardiac development. Our data show that zebrafish holds
103 potential as a model to study PERK function in developmental disorders, such as WRS.
104

105 ## 2. Material and Methods

106

107 ### 2.1 Drugs, solvents, and solutions

108 Stock solutions of the PERK inhibitor GSK2606414 (Merck Millipore, 516535) [15, 18], the
109 muscle relaxant D-tubocurarine (dTC; Sigma, T2379), and the anesthetic tricaine
110 methanesulfonate (0.02%; Sigma, E10521) were prepared in DMSO (Sigma, 276855) and
111 diluted in standard E3 medium [19]. DMSO levels were kept under 0.2% [20].

112

113 ### 2.2 Zebrafish maintenance and husbandry

114 Adult AB strain zebrafish were supplied by the Interdisciplinary Centre of Marine and
115 Environmental Research (CIIMAR, Portugal), transgenic strains of zebrafish were obtained
116 from José Bessa's laboratory at the Institute for Research and Innovation in Health (i3s,
117 University of Porto, Portugal). Zebrafish adults were maintained at 28 ± 1°C on a 14 h:10 h
118 light:dark cycle [21, 22]. Breeding pairs (1:1, male:female) were placed in breeding tanks on
119 the day before egg collection. Ninety minutes after starting the light period, eggs were
120 collected, and time point was recorded as 0 h post fertilization (hpf). **Ethic statement:**
121 Handling of zebrafish followed the European Directive 2010/63/EU and the Portuguese Law
122 (Decreto-Lei 113/2013). Experiments were performed according to the 3Rs principle by
123 reducing the number of animals used and using refined techniques that reduce animal suffering,
124 using procedures approved by the i3S Animal Welfare Body.

125

126 ### 2.3 Drug treatments

127 5 zebrafish/well were randomly distributed in 24-well plates (0.5 mL E3/well) and kept at 28
128 ± 1°C on a 14 h:10 h light: dark cycle throughout the assay. Zebrafish were continuously

129 exposed to GSK2606414 or solvent (DMSO) from 4 to 76 hpf and solutions were renewed
130 daily [21]. dTC was incubated for 10 minutes before assays endpoint (≥ 15 zebrafish).
131

132 **2.4 Brightfield microscopy**

133 For brightfield microscopy, we used a stereomicroscope (Stemi DV4, Zeiss, Göttingen,
134 Germany) or an inverted microscope (Eclipse TE300, Nikon, Tokyo, Japan). The inverted
135 microscope was attached to a motorized stage (ProScan, Prior) and a CCD camera (ORCA-
136 ER, Hamamatsu), constituting a Nikon-Prior-Hamamatsu (NPH) imaging system that was
137 controlled by the open-source software Micro-Manager (v. 2.0; https://micro-manager.org):

138 2.4.1 ***Monitoring zebrafish development:*** Zebrafish were scored as normal,
139 abnormal, or dead; hatched (ruptured chorion and free tail movement) or unhatched at
140 28, 52 and 76 hpf. Death was ascertained according to OECD guideline 236 [23],
141 normal development as previously described [24], and abnormalities as cardiac and
142 skeletal (further into scoliosis, curly-up tail, or kyphosis). Dead zebrafish were removed
143 at each time point and only live ones were used in subsequent assays.

144 **2.4.2** ***Morphometric analysis:*** Zebrafish body length was measured from the tip of
145 the head (between the eyes) to the end of the tail [25] and trunk-tail angle was measured
146 at the intersection between the rostral (trunk) and caudal (tail) notochord at the level of
147 the anus (Figure 3 B).

148 2.4.3 ***Heartbeat and atrio-ventricular coordination:*** Heartbeats were counted in 4
149 zebrafish per condition, per experiment, during 20 s, at 72-80 hpf [26]. Atrio-
150 ventricular coordination recordings were obtained with "Plot Z-axis profile" on ImageJ
151 after imaging zebrafish for 90 seconds at 12 frames per second.

152 2.4.4 ***Tail coilings:*** Spontaneous activity was measured at 28 hpf in glass bottom 96-
153 well plates where each zebrafish was imaged for 3 minutes at a frequency of 4.5 frames
154 per second and 2x2 or 4x4 binning [19].
155 **2.4.5** ***Birefringence analysis:*** 76 hpf zebrafish were anesthetized, immobilized on a
156 glass surface, oriented laterally, and illuminated with linearly polarized light (Screen-
157 Tech, ST-38). An orthogonal polarization filter was placed after the samples to block
158 directly transmitted light. Thus, only light whose polarization angle is affected by the
159 sample is collected by the NPH imaging system [27]. Pixel intensity in the trunk region
160 was measured by selecting the region of interest with ImageJ software.
161
162 **2.5 Touch-evoked escape response**
163 At 76 hpf, at least 6 zebrafish/condition were submitted to 10 alternate touches to the head and
164 to the tail with 10 µL pipette tip with a recovery time of 30 seconds [28]. Data are presented as
165 response rates in percentage of total touches.
166
167 **2.6 Fluorescent microscopy**
168 Zebrafish were imaged with the NPH system coupled to a monochromator (Polychrome II,
169 Photonics) as follows.
170 **2.6.1** ***2-NBDG labelling:*** 3 hours before 76 hpf end-point, zebrafish were incubated
171 with a fluorescent glucose analogue - 600 µM 2-NBDglucose (2-(7-Nitro-2,1,3-
172 benzoxadiazol-4-yl)-D-glucosamine) (Tebu-Bio,10-1459) [29, 30]; and a positive
173 control for neuromast labelling - Mitotracker Deep Red (1 µM, Invitrogen, M22426,
174 labels polarized mitochondria in neuromasts) in 96 well plates (4 zebrafish /well). At
175 76 hpf, each zebrafish was anesthetized and imaged in a glass-bottom chamber. 2-
176 NBDglucose was excited at 475 nm and Mitotracker Deep Red at 650 nm for 1 second.

177 Emissions were collected using band pass filters (Chroma 69008 – ET –
178 ECFP/EYFP/mCherry) with a 10 × objective. Images of the entire fish were stitched
179 with the GNU image manipulation program (The GIMP Development Team, 2019;
180 https://www.gimp.org), before evaluation of anterior and posterior neuromasts [31].
181 **2.6.2** ***Transgenic zebrafish:*** Double transgenic zebrafish expressing GFP in insulin-
182 producing β cells and mCherry in somatostatin-producing δ cells (Tg(ins:GFP,
183 sst:mCherry)) or in elastase-producing cells (Tg(ins:GFP, ela:mCherry)) were kept in
184 24-well plates (5 zebrafish/plate) with E3 media. We used two pharmacological
185 approaches: 1) GSK2606414 exposure from 4 hpf (before the principal islet of
186 Langerhans is formed within the endocrine pancreas) to 28, 76 or 148 hpf; 2)
187 GSK2606414 exposure from 76 hpf (when the principal islet is already formed) to 148
188 hpf [32]. At the final time point (28, 76 or 148 hpf) zebrafish were anesthetized by rapid
189 cooling on ice and fixed in 4% paraformaldehyde overnight. GFP was excited at 488
190 nm and mCherry was excited at 575 nm. Emissions were collected using band pass
191 filters (Chroma 59022 – EGFP/mCherry) with a 20 × objective. The area of GFP- or
192 mCherry-labelled pancreas in each image was assessed with the ImageJ software
193 (https://imagej.nih.gov/ij).
194
195 **2.8 Western blot**
196 24-27 zebrafish larvae were rinsed with ice-cold water twice before being placed in RIPA
197 buffer (50 mM Tris (NZYTech, MB01601), 150 mM NaCl (Merck, S9888), 1 mM EDTA
198 (Sigma-Aldrich, E6758), 1% IGEPAL CA-630 (Sigma-Aldrich, I3021), 1% sodium
199 deoxycholate (Sigma-Aldrich, D6750), 0.1% sodium dodecyl sulfate (Sigma-Aldrich, L3771)
200 supplemented with a protease and phosphatase inhibitor cocktail (Thermo Scientific, 78440).
201 After 3 freeze-thaw cycles, homogenization with Precellys Evolution (6800 rpm, 5 × 42 s with

202 37 s interval) and centrifugation at 12,000 × g (10 min, 4 °C), supernatant protein
203 concentrations were quantified by the Bradford method. 30 to 40 µg of protein extracts were
204 supplemented with Bolt LDS sample buffer (Invitrogen, B0007) and Bolt sample reducing
205 agent (Invitrogen, B0009), denatured at 95 ºC for 5 min, and loaded into 4–15% Mini-
206 PROTEAN TGX™ Precast Protein Gels (Biorad, 4561084), which were electrophoresed (125
207 and 200 V, 30 min) and wet-transferred to PVDF membranes (Millipore, IPVH00010)
208 overnight (30 V, 4ºC). Membranes were blocked (1 h, room temperature or overnight at 4ºC)
209 with 5% bovine serum albumin (BSA, NZYTech, MB04602) in PBS with 0.05% Tween 20
210 (PBST) and incubated with primary antibodies (Supplementary Table 1). After washing with
211 PBST, membranes were incubated with respective horseradish peroxidase-conjugated
212 secondary antibodies (1 h) (Supplementary Table 2), for detection with a Chemiluminescent
213 kit (Novex ECL, Invitrogen, WP20005) and a ChemiDoc MP Imaging system (Bio-Rad).
214 Membrane Coomassie (Sigma-Aldrich, 27816) staining was used for loading control rather
215 than 'housekeeping' proteins, as their levels may change under certain conditions [33].
216 Densitometric analyses were performed with the Image J software. In each independent
217 experiment, samples from control (0 µM GSK) and 10 µM GSK- treated zebrafish were run in
218 the same gel.
219
220 **2.9 Bioinformatic analyses**
221 **2.9.1 Comparison of PERK orthologues**
222 Protein sequence data from zebrafish (*Danio rerio,* XP_005156642.2), human (*Homo*
223 *sapiens,* AAI26357.1), mouse (*Mus musculus,* AAH54809.1), and fruit fly (*Drosophila*
224 *melanogaster,* AAF61200.1) were obtained from UniProt (https://www.uniprot.org/,
225 28th February 2025). The amino acid sequences from the total human PERK protein and
226 from its kinase domain were compared with its orthologue proteins from zebrafish,

227 mouse, and fruit fly, using the Protein BLAST tool
228 (https://blast.ncbi.nlm.nih.gov/Blast.cgi). Additionally, we determined the identity of
229 the vital amino acids for GSK2606414 binding to the catalytic site of PERK, by aligning
230 the protein sequence from zebrafish and human.

231 **2.9.2 Zebrafish PERK 3D structure and molecular docking**

232 The predicted three-dimensional protein structures of zebrafish PERK (UniProt:
233 B8JI14) and human PERK (UniProt: Q9NZJ5) were obtained from AlphaFold Protein
234 Structure Database [34, 35]. UCSF ChimeraX software was used to visualize, align
235 (Matchmaker tool) and calculate the root-mean-square deviation (RMSD) of the three-
236 dimensional structures of human PERK (PDB: 4g31) and zebrafish PERK (UniProt:
237 B8JI14), and GSK2606414.

238

239 **2.10 Statistical Analyses**

240 Data are shown as mean ± standard error of the mean (SEM) of the *n* specified in figure legends.
241 For experiments with only two groups, comparisons were made with Student's *t*-test. For
242 single-factor (drug concentration) comparisons of multiple groups to their respective control,
243 we used One-Way ANOVA with Dunnett's *post-hoc* test. For two-factor (drug concentration
244 vs. time) analysis, we used Two-Way ANOVA with Sidak's *post-hoc* test. For survival analysis
245 we used the Mantel-Cox (Log-rank) test. $P < 0.05$ was taken as statistically significant. Data
246 analyses were performed with Prism 6.0 (GraphPad).

247 **3. Results**

248

249 **3.1 The PERK-GSK2606414 binding site is conserved in humans and zebrafish**

250 To assess the potential of zebrafish to study PERK function and its pharmacological
251 modulation, we performed bioinformatic comparisons of the amino acid and structural identity
252 of zebrafish and human PERK, including specifically the binding site for the PERK inhibitor
253 GSK2606414. We selected GSK2606414 (hereafter GSK; not to be confused with glycogen
254 synthase kinase) because: it is one of the most used PERK inhibitors [1]; it was previously used
255 in zebrafish [15]; and the vital amino acids for its binding to PERK are identified [36, 37].

256 The zebrafish PERK homologue presented 59% global amino acid identity with human
257 PERK (Figure 1 A). Using Protein BLAST, we observed that out of the 12 vital amino acids
258 for GSK binding to PERK [36, 37], there is only one difference between human and zebrafish
259 (Figure 1 B). Such difference is a valine in human vs. isoleucine in zebrafish, and both amino
260 acids are hydrophobic. Using molecular visualization with ChimeraX, we observed that the
261 average distance between the 3D structures of zebrafish and human PERK is under 1 Å (Figure
262 1 C, D), indicating high similarity [38].

263 These results predict a high probability of GSK binding and inhibiting zebrafish PERK.
264 To test such prediction, we proceeded with functional assays.

265

266 **3.2 The PERK inhibitor GSK2606414 is bioactive in zebrafish**

267 To evaluate the effects of PERK inhibition, we evaluated the survival and hatching of zebrafish
268 treated with increasing concentrations of GSK over time (Figure 2 A). We observed a time-
269 dependent decrease in survival, with 10 μM GSK being the concentration that induces a
270 significant effect (50%) at 76 hpf (Figure 2 B). For zebrafish that survived GSK, hatching
271 increased time-dependently, without significant differences across GSK concentrations (Figure

272 2 C). Next, we assessed the effect of GSK on the levels of PERK pathway (ISR) biomarkers in
273 the zebrafish at 76 hpf using western blot (Figure 2 D *i*). Treatment with GSK (10 μM, 72h)
274 significantly decreased levels of phosphorylated eIF2α, ATF4, and CHOP (Figure 2 D *ii-vi*).
275 Together, GSK effects confirm its bioactivity and are compatible with PERK pathway
276 inhibition as previously reported [15].
277
278 **3.3 PERK inhibition induces morphologic defects in zebrafish**
279 PERK loss-of function elicits skeletal dysplasia in patients [5]. To investigate the role of PERK
280 in skeletal development, we exposed zebrafish embryos to the PERK inhibitor from 4 to 76 hpf
281 and monitored their development over time. GSK (10 μM) evoked a significant time-dependent
282 increase in morphological defects (Figure 3 A *i*). The most common defect was a curly-up tail
283 and a few cases of scoliosis (Figures 3 A *ii* - *iv*). Exposure to GSK (10 μM) caused 20 ± 5
284 degrees change in the zebrafish trunk-tail angle at 76 hpf (Figure 3 B) and a significant decrease
285 in body length (Figure 3 C).
286 To ascertain if the morphological defects evoked by GSK originate primarily in
287 developing skeletal or muscular structures, we tested if the defects could be reversed by a
288 muscle relaxant (d-tubocurarine; dTC; antagonist of muscular nicotinic receptors [39];
289 effective in zebrafish [40]). We observed a concentration-dependent decrease in escape
290 responses, with a maximal relaxation effect at 3 mM (Figure 3 D *i,ii*), confirming dTC efficacy
291 as previously described [40]. 3 mM dTC did not recover trunk-tail angle in GSK-treated
292 zebrafish (Figure 3 E), indicating that that abnormal skeletal development, rather than muscle
293 contraction, is the main cause of the morphological defects.
294 We measured otolith area (Supplementary Figure 1) and eye/body ratio (Supplementary
295 Figure 2) as negative controls (unrelated with WRS phenotypes) and found no changes upon
296 GSK exposure indicating that GSK effects on zebrafish morphology are selective.

297 These results indicate that upon PERK inhibition, zebrafish presented abnormal skeletal
298 development and growth retardation, indicating that this small vertebrate holds potential to
299 study the role of PERK in skeletal development.
300

301 **3.4 PERK inhibition delays endocrine pancreas development and limits glucose uptake**
302 **in zebrafish**

303 Lack of PERK in WRS patients leads to decreased β-cell mass, impaired insulin production
304 and neonatal diabetes [41, 42]. Exocrine pancreas dysfunction was found in only 10.6% of
305 patients [43, 44]. Thus, we explored if zebrafish could be useful to study PERK's role in
306 pancreatic development.

307 To ascertain the effects of PERK inhibition in exocrine and endocrine pancreas
308 development, we used two transgenic zebrafish lines expressing GFP in insulin-producing β-
309 cells (Figure 4 A): one line also expressed mCherry in somatostatin-producing δ-cells from the
310 endocrine pancreas – Tg(*ins:GFP, sst:mCherry*); the other line expressed mCherry in elastase-
311 producing exocrine pancreas –Tg(*ins:GFP, ela:mCherry*). We exposed both lines to GSK (10
312 μM) and measured the GFP/mCherry labelled areas as proxies for cell mass.

313 To test if the effects of GSK inhibition were selective for the early embryo
314 development, we used two exposure protocols: the *early exposure protocol* (Figure 4 B *i*)
315 started before the formation of the first Langerhans islet (endocrine pancreas); the *late exposure*
316 *protocol* started after islet formation (Figure 4 B *ii*). Early PERK inhibition (4 hpf) delayed
317 development of the endocrine pancreas, significantly decreasing β and δ cell mass at 28 hpf,
318 which seems to recover overtime (Figure 4 C *i*, D *i*). Late inhibition (76 hpf) failed to alter
319 endocrine cell mass (Figure 4 C *ii*, D *ii*). Regarding the exocrine pancreas mass, *ela:mCherry*
320 fluorescence was only detectable at 148 hpf, and remained unchanged with either early or late

321 GSK exposure protocols (Figure 4 E). These findings support the hypothesis that PERK
322 inhibition delays the early embryonic development of the endocrine pancreas.
323 To test if delayed endocrine development affected glucose homeostasis, we measured
324 the uptake of the fluorescent glucose probe 2-NBDglucose [29] in zebrafish treated with GSK
325 from 4 to 76 hpf (early exposure protocol). 2-NBDglucose uptake was measured in neuromast
326 cells, given their direct exposure to probes in the external media, using Mitotracker Deep Red
327 as a positive control for neuromast staining. Early PERK inhibition significantly decreased the
328 uptake of 2-NBDglucose (Figure 5 A, B), indicating that PERK inhibition, induces a diabetic-
329 like phenotype in zebrafish.
330
331 **3.5 PERK inhibition evokes neuromuscular and cardiac impairments in zebrafish**
332 Beyond diabetes and skeletal dysplasia, patients with loss-of-function mutations in PERK may
333 also present impaired brain development [45], muscle weakness [46] and cardiac alterations
334 [47, 48]. We first assessed the role of PERK on zebrafish neuromuscular function by measuring
335 spontaneous tail-coiling and touch-evoked escape responses upon PERK inhibition [49-51].
336 GSK (10 μM) significantly increased tail-coiling events in early development (28 hpf embryos
337 inside the chorion; Figure 6 A) and significantly decreased escape responses in later
338 development (76 hpf larvae; Figure 6 B). To test for altered muscle integrity, we assessed the
339 arrangement of sarcomeres by measuring how well they diffracted polarized light
340 (birefringence assay) [52] (Figure 6 C *i*). Treatment with 10 μM GSK significantly decreased
341 muscle birefringence intensity (Figure 6 C *ii, iii*).
342 Next, we monitored cardiac morphology and function in PERK-inhibited zebrafish, where
343 10 μM GSK induced a time-dependent increase in pericardial oedema (Figure 7 A).
344 Additionally, at 76 hpf, 10 μM GSK induced bradycardia without altering atrio-ventricular
345 coordination in zebrafish (Figure 7 B).

346 These results suggest that PERK-inhibited zebrafish present neuromuscular and cardiac
347 abnormalities in morphology and function, indicating that zebrafish are suitable models to
348 study PERK effects on neuromuscular and cardiac development and function.
349
350
351 **4. Discussion**
352 This study contributes to the understanding of PERK's role in the embryonic development of
353 zebrafish, building on PERK's functions in zebrafish sleep and oxidative stress regulation [15-
354 17]. We show that PERK inhibition causes defective skeletal development and diabetic-like
355 phenotypes, cardiac and neuromuscular alterations in zebrafish, mirroring the clinical features
356 of Wolcott-Rallison syndrome patients. These results highlight the potential of zebrafish to
357 study PERK's role in developmental diseases with multisystem involvement such as the WRS.
358 PERK inhibition with GSK2606414 (GSK), one of the most used PERK inhibitors in
359 the scientific literature, decreased ISR activation in animals like mice [53], frogs [54] and flies
360 [15]. In the present study, we show that GSK decreases the levels of ISR markers in zebrafish,
361 which suggests that GSK is bioactive and effective in decreasing PERK pathway activity.
362 Additionally, GSK evoked key WRS-associated phenotypes (impaired skeletal development
363 and diabetic-like phenotype), while sparing non-WRS-associated parameters as otolith area
364 and eye/body ratio. Although we cannot exclude GSK off-targeting c-KIT and RIPK kinases
365 [55, 56], zebrafish with genetically inhibited KITa/b and RIPK3 [57, 58] did not show the
366 curly-up tail and other structural alterations reported in our study, suggesting that such
367 alterations are not off-targets effects of GSK in c-KIT and RIPK kinases. Thus, these results
368 are compatible with GSK selectively inhibiting PERK in zebrafish.
369 Loss of PERK function causes growth retardation and skeletal dysplasia in humans [5] and
370 mice, via impairments in collagen secretion, osteoblast differentiation and bone mineralization

371 [9, 59, 60]. Here, we show that PERK inhibition in zebrafish causes growth retardation and
372 spinal deformities resistant to muscle relaxation with tubocurarine. Since at the time of the
373 assays (76 hpf) the zebrafish cartilage is starting to ossify [61], our findings indicate that PERK
374 inhibition impairs zebrafish skeletal development.

375 PERK controls pancreatic β-cell development and insulin production [62]. Loss of PERK
376 function in humans and mice causes decreased pancreatic mass and neonatal diabetes, by
377 impairing β-cell proliferation and proinsulin maturation in the endoplasmic reticulum [63-66].
378 Here we show that PERK inhibition during early zebrafish development delays endocrine
379 pancreas formation, resulting in a decreased β-cell mass, which gradually recovers overtime.
380 To assesses whether insulin homeostasis is impaired in PERK-inhibited zebrafish we used a
381 surrogate indicator [67]. We found reduced 2-NBDglucose uptake, which indicates that insulin
382 homeostasis remains partly compromised despite the ongoing β-cell mass recovery. Such
383 recovery in the presence of GSK suggests that zebrafish can regenerate pancreatic tissue [68,
384 69] by PERK-independent mechanisms. The identification of such PERK-independent
385 mechanisms in zebrafish may assist the development of novel therapies for β-cell regeneration
386 for human diabetes [70].

387 In contrast to the delayed development of the zebrafish endocrine pancreas, we found no
388 effect of PERK-inhibition upon the mass of the exocrine pancreas. While different mechanisms
389 regulate development of the endocrine and exocrine pancreas [43, 65], we cannot exclude that
390 extended exposure of zebrafish to the PERK inhibitor may alter the mass of the exocrine
391 pancreas. Future studies using selective PERK knockout in zebrafish pancreatic cell sub-types
392 may contribute to understand differential pancreatic vulnerability.

393 Beyond pancreatic dysfunction, PERK inhibition in humans and mice impairs neuronal
394 and muscular functions [5, 6, 11, 71, 72]. Here we show that PERK inhibition in zebrafish
395 increases spontaneous tail movements early in development, which arise in a spinal central

396 pattern generator that provides rhythmic depolarizations [49, 51], and decreases touch-evoked
397 escape responses later in development, which arise in sensory neurons [50, 51]. We also show
398 that PERK-inhibited zebrafish display altered muscular integrity, likely contributing to
399 decreased escape responses. Thus, as with mammals, the mechanisms underlying motor
400 impairment in PERK-inhibited zebrafish combine dysfunctions in neurons and muscle.

401 Patients and mice with PERK loss of function often display cardiac malformations [10,
402 47, 48]. Here we show that PERK-inhibited zebrafish display cardiac abnormalities, such as
403 oedema and bradycardia. The transparency and small size of young zebrafish is amenable to
404 the detection of cardiac abnormalities that would be fatal in larger animals due to insufficient
405 oxygen diffusion [73]. Moreover, zebrafish may assist discovery of heart regeneration
406 mechanisms [74]. Thus, future studies with a more detailed structural and functional
407 characterization of the cardiac abnormalities in PERK-inhibited or deleted zebrafish, may
408 provide valuable insights into disease mechanisms and potential therapeutics.

409

410 **5. Conclusions**

411 This study highlights the potential of the small vertebrate zebrafish as a model for
412 developmental diseases, namely those caused by PERK inhibition like the WRS. We show that
413 pharmacological inhibition of PERK with GSK2606414 mimicked WRS pathophysiology by
414 inducing defective growth and skeletal development, and diabetic-like phenotypes such as
415 delayed development of the endocrine pancreas and altered glucose homeostasis. PERK
416 inhibition also impaired neuromuscular and cardiac development, while sparing non-WRS
417 associated parameters like otolith area and eye/body ratio. Future studies using CRISPR/Cas9
418 technology can be used to generate zebrafish models with conditional/selective expression of
419 human PERK with WRS-driving mutations [75]. Also, future research on the mechanisms
420 governing PERK-independent pancreatic regeneration in zebrafish may uncover potential

421 therapeutic targets for diabetes. Further, the scalability of zebrafish models holds great
422 potential to enhance the efficiency of drug screening against PERK-associated developmental
423 diseases.

Declarations

CRediT authorship contribution statement

Liliana M. Almeida: Conceptualization, Methodology, Investigation, Validation, Data curation, Visualization, Formal analysis, Writing – original draft, Writing – review and editing; **Leonor Pereira Lima:** Investigation, Validation, Formal analysis, Visualization, Writing – review and editing; **Nuno A. S. Oliveira:** Investigation, Methodology, Validation, Visualization, Formal analysis, Writing – review and editing; **Rui F. O. Silva:** Investigation, Validation, Formal analysis; **Bruno Sousa:** Investigation, Validation; **José Bessa:** Methodology, Resources, Writing – review and editing, Funding acquisition; **Brígida R. Pinho:** Conceptualization, Methodology, Writing – review and editing, Supervision; **Jorge M. A. Oliveira:** Conceptualization, Methodology, Resources, Writing – review and editing; Funding acquisition, Project administration, Supervision.

Funding

JMAO's laboratory - FCT – Fundação para a Ciência e a Tecnologia, Portugal – (UIDB/04378/2020; UIDP/04378/2020; LA/P/0140/2020). LMA - FCT PhD fellowship - SFRH/BD/138451/2018. BRP - FCT funding program DL57/2016 - Norma transitória (DL57/2016/CP1346/CT0016). JB's laboratory - FCT project PTDC/BIA-MOL/3834/2021. JB's FCT contract CEECIND/03482/2018.

Conflict of interest statement

No financial or non-financial interests to disclose.

Figure legends

449 **Figure 1.** Bioinformatic analyses of PERK identity and GSK2606414-binding in human vs.
450 zebrafish. (**A**) Percentage of identity between human, fruit fly (*Drosophila melanogaster*),
451 zebrafish (*Danio rerio*), and mouse (*Mus musculus*) PERK (total and kinase domain); Protein
452 BLAST. (**B**) Comparing vital GSK2606414 (GSK)-binding amino acids in the catalytic domain
453 of human and zebrafish PERK. Valine 651 in human (yellow) is substituted by the also
454 hydrophobic Isoleucine 671 (red) in zebrafish; Protein BLAST. (**C**) Predicted GSK (purple, #)
455 binding to human (light blue) and zebrafish (dark blue) PERK; ChimeraX. (**D**) Root Mean
456 Square Deviation (RMSD) comparing human and zebrafish PERK tertiary structures and
457 respective reference values; ChimeraX.
458
459 **Figure 2.** GSK2606414 effects on zebrafish survival, hatching, and PERK pathway
460 biomarkers. (**A**) Experimental timeline. (**B**) Zebrafish survival when exposed to GSK2606414
461 (GSK; 0-10 μM) over time (4-76 hours post-fertilization; hpf); n = 50-234 zebrafish, 5
462 independent breedings, Mantel-Cox test for survival, $^{*}P < 0.05$ vs. 0 μM GSK (control). (**C**)
463 Hatching of zebrafish treated with GSK; n= 50-234 zebrafish, 5 breedings, Two-Way ANOVA,
464 time effect: $^{\#}P < 0.05$. (**D**) Western blot of live 76 hpf zebrafish: *i*) Schematic representation
465 of the PERK pathway biomarkers; *ii-vi*) Representative blots and quantifications; n = 4
466 independent experiments (pool of 24-27 larvae per condition and per experiment); *t*-test: $^{*}P <$
467 0.05.
468
469 **Figure 3.** GSK2606414 impaired skeletal development in zebrafish. (**A**) (*i*) Morphological
470 defects following GSK2606414 (GSK) (0-10 μM) treatment overtime; $^{*}P < 0.05$, 10 vs. 0 μM
471 GSK; $^{\#}P<0.05$, effect of time for 10 μM GSK, Two-Way ANOVA with Sidak *post-hoc*; n =
472 50-234 zebrafish; 5 independent experiments. (*ii-v*) Proportion of curly-up tail and scoliosis at
473 76 hpf, and representative images. (**B, C**) Measurements (blue lines) and quantifications of

474 trunk-tail angle and body length at 76 hpf; *$P < 0.05$ vs 0 μM GSK, One-Way ANOVA with
475 Dunnett's *post-hoc*; $n = 15$ zebrafish, 3 independent experiments. (**D**) Effect of muscle relaxant
476 d-tubocurarine (dTC, 0.03–3 mM) on escape responses after head or tail touch at 76 hpf; Grey
477 bands are mean ± SEM for control zebrafish; *$P < 0.05$ vs 0 mM dTC, One-Way ANOVA with
478 Dunnett's *post-hoc, n* = 15 zebrafish, 3 independent experiments. (**E**) (*i-iv*) Representative
479 images of zebrafish for the indicated-treatments. (*v*) Quantification of zebrafish with
480 morphological defects at 76 hpf for the indicated treatments. *$P < 0.05$ vs control, One-Way
481 ANOVA with Sidak's *post-hoc*, $n = 15$ zebrafish; 3 independent breedings. Blue arrows: curly-
482 up tail.
483
484 **Figure 4.** Pancreatic development in transgenic zebrafish. **(A)** Representative images of normal
485 pancreas development in Tg(*ins:GFP, sst:mCherry*) and Tg(*ins:GFP, ela:mCherry*) zebrafish.
486 (**B)** early (*i*) and late (*ii*) GSK2606414 (GSK)-exposure protocols. (**C-E**) Area measurements
487 for *ins:GFP* (green, insulin-producing β-cells), *sst:mCherry* (red, somatostatin-producing δ-
488 cells), and *ela:mCherry* (red, elastase-producing exocrine cells), in zebrafish exposed to 10 μM
489 GSK since 4 hpf (*i*, early exposure) or since 76 hpf (*ii*, late exposure). *$P < 0.05$, *t*-test, $n = 4$-
490 33 larvae. Representative images of GFP and mCherry are shown below respective bars. Scale
491 bars indicate 200 μm.
492
493 **Figure 5.** GSK2606414 effects on 2-NBDglucose uptake in zebrafish. (**A**) Representative
494 brightfield and fluorescence images of zebrafish at 76 hpf, following treatment with (*i*) 0 μM
495 (control) or (*ii*) 10 μM GSK2606414 since 4 hpf. Images show functional labelling at 76 hpf
496 with the fluorescent glucose analogue 2-NBDglucose (2-NBDG) for neuromasts that uptake
497 glucose, and with MitoTracker Deep Red that labels mitochondria in neuromasts as positive
498 control. In the "Merge" images, yellow circles highlight neuromasts with both 2-NBDglucose

499 and MitoTracker, while red circles highlight those containing MitoTracker only. Below, 2x
500 amplified images show neuromasts from the zebrafish lateral line, with arrows indicating
501 neuromasts on the side proximal to the microscope objective (the paired neuromasts on the
502 opposite side are unmarked). (**B**) Quantification of neuromasts labelled with 2-NBDglucose.
503 *$P < 0.05$, t-test, n = 9-12 zebrafish per condition.
504
505 **Figure 6.** GSK2606414 effects on neuromotor responses and muscle integrity. (**A**) (*i*)
506 Representative tail coiling time-lapse: white line highlights notochord movement. (*ii*)
507 Quantification of tail coiling in 28 hpf zebrafish treated with GSK2606414 since 4 hpf; n = 23-
508 26 zebrafish. (**B**) Quantification of escape responses after head (*i*) or tail (*ii*) touches at 76 hpf;
509 n = 13-114 zebrafish. (**C**) (*i*) Schematic representation of the birefringence assay for muscle
510 integrity; (*ii*) Representative images of muscle birefringence at 76 hpf. (*iii*) Quantification of
511 birefringence intensity; n = 15 zebrafish. (**A-C**) Grey bands are mean ± SEM for 0 μM GSK
512 (control); *$P < 0.05$ vs. (control), One-Way ANOVA with Dunnett's *post-hoc*.
513
514 **Figure 7.** GSK2606414-induced morphological and functional cardiac defects. (**A**) (*i*)
515 Quantification of live zebrafish with pericardial oedema at the indicated hpf and GSK
516 concentrations. *$P < 0.05$, 10 vs. 0 μM GSK (control); Two-Way ANOVA with Sidak *post-*
517 *hoc* n= 50-234 zebrafish; 5 independent experiments. (*ii,iii*) Representative images of zebrafish
518 treated with GSK vs. control; blue arrow: pericardial oedema. (**B**) (*i*) Heartbeats per minute
519 (bpm) of 76 hpf zebrafish exposed to increasing GSK concentrations since 4 hpf; Grey band is
520 mean ± SEM for control; *$P < 0.05$ vs control, One-Way ANOVA with Dunnett's *post-hoc*, n
521 = 13-116 zebrafish; (*ii*) Representative images of the heart and plots of atrio-ventricular
522 coordination in control and 10 μM GSK-treated zebrafish (a: atrium – red; v: ventricle – blue).
523

524 **References**

525

526 [1] L.M. Almeida, B.R. Pinho, M.R. Duchen, J.M.A. Oliveira, The PERKs of mitochondria
527 protection during stress: insights for PERK modulation in neurodegenerative and metabolic
528 diseases, Biol Rev Camb Philos Soc, (2022).

529 [2] L. Peshkin, M. Wuhr, E. Pearl, W. Haas, R.M. Freeman, Jr., J.C. Gerhart, A.M. Klein, M.
530 Horb, S.P. Gygi, M.W. Kirschner, On the Relationship of Protein and mRNA Dynamics in
531 Vertebrate Embryonic Development, Dev Cell, 35 (2015) 383-394.

532 [3] P. Wang, J. Li, J. Tao, B. Sha, The luminal domain of the ER stress sensor protein PERK
533 binds misfolded proteins and thereby triggers PERK oligomerization, J Biol Chem, 293 (2018)
534 4110-4121.

535 [4] V. Senee, K.M. Vattem, M. Delepine, L.A. Rainbow, C. Haton, A. Lecoq, N.J. Shaw, J.J.
536 Robert, R. Rooman, C. Diatloff-Zito, J.L. Michaud, B. Bin-Abbas, D. Taha, B. Zabel, P.
537 Franceschini, A.K. Topaloglu, G.M. Lathrop, T.G. Barrett, M. Nicolino, R.C. Wek, C. Julier,
538 Wolcott-Rallison Syndrome: clinical, genetic, and functional study of EIF2AK3 mutations and
539 suggestion of genetic heterogeneity, Diabetes, 53 (2004) 1876-1883.

540 [5] C. Julier, M. Nicolino, Wolcott-Rallison syndrome, Orphanet J Rare Dis, 5 (2010) 29.

541 [6] J. Bruch, C. Kurz, A. Vasiljevic, M. Nicolino, T. Arzberger, G.U. Hoglinger, Early
542 Neurodegeneration in the Brain of a Child Without Functional PKR-like Endoplasmic
543 Reticulum Kinase, J Neuropathol Exp Neurol, 74 (2015) 850-857.

544 [7] A.G. Tzakis, M.J. Nunnelley, A. Tekin, L.D. Buccini, J. Garcia, K. Uchida, H.L. Neville,
545 M.A. Nares, P. Ruiz, O. Bodamer, Liver, pancreas and kidney transplantation for the treatment
546 of Wolcott-Rallison syndrome, Am J Transplant, 15 (2015) 565-567.

547 [8] H.P. Harding, H. Zeng, Y. Zhang, R. Jungries, P. Chung, H. Plesken, D.D. Sabatini, D.
548 Ron, Diabetes mellitus and exocrine pancreatic dysfunction in perk-/- mice reveals a role for
549 translational control in secretory cell survival, Mol Cell, 7 (2001) 1153-1163.
550 [9] P. Zhang, B. McGrath, S. Li, A. Frank, F. Zambito, J. Reinert, M. Gannon, K. Ma, K.
551 McNaughton, D.R. Cavener, The PERK eukaryotic initiation factor 2 alpha kinase is required
552 for the development of the skeletal system, postnatal growth, and the function and viability of
553 the pancreas, Mol Cell Biol, 22 (2002) 3864-3874.
554 [10] T. Shimizu, K. Maruyama, T. Kawamura, Y. Urade, Y. Wada, PERK participates in
555 cardiac valve development via fatty acid oxidation and endocardial-mesenchymal
556 transformation, Sci Rep, 10 (2020) 20094.
557 [11] Y.S. Gallot, K.R. Bohnert, A.R. Straughn, G. Xiong, S.M. Hindi, A. Kumar, PERK
558 regulates skeletal muscle mass and contractile function in adult mice, FASEB J, 33 (2019)
559 1946-1962.
560 [12] M.A. Trinh, H. Kaphzan, R.C. Wek, P. Pierre, D.R. Cavener, E. Klann, Brain-specific
561 disruption of the eIF2alpha kinase PERK decreases ATF4 expression and impairs behavioral
562 flexibility, Cell Rep, 1 (2012) 676-688.
563 [13] T. Teame, Z. Zhang, C. Ran, H. Zhang, Y. Yang, Q. Ding, M. Xie, C. Gao, Y. Ye, M.
564 Duan, Z. Zhou, The use of zebrafish (Danio rerio) as biomedical models, Anim Front, 9 (2019)
565 68-77.
566 [14] T.Y. Choi, T.I. Choi, Y.R. Lee, S.K. Choe, C.H. Kim, Zebrafish as an animal model for
567 biomedical research, Exp Mol Med, 53 (2021) 310-317.
568 [15] S. Ly, D.A. Lee, E. Strus, D.A. Prober, N. Naidoo, Evolutionarily Conserved Regulation
569 of Sleep by the Protein Translational Regulator PERK, Curr Biol, 30 (2020) 1639-1648 e1633.

570 [16] B. Jin, L. Xie, D. Zhan, L. Zhou, Z. Feng, J. He, J. Qin, C. Zhao, L. Luo, L. Li, Nrf2
571 dictates the neuronal survival and differentiation of embryonic zebrafish harboring
572 compromised alanyl-tRNA synthetase, Development, 149 (2022).
573 [17] K. Mukaigasa, T. Tsujita, V.T. Nguyen, L. Li, H. Yagi, Y. Fuse, Y. Nakajima-Takagi, K.
574 Kato, M. Yamamoto, M. Kobayashi, Nrf2 activation attenuates genetic endoplasmic reticulum
575 stress induced by a mutation in the phosphomannomutase 2 gene in zebrafish, Proc Natl Acad
576 Sci U S A, 115 (2018) 2758-2763.
577 [18] S.R. Stockwell, G. Platt, S.E. Barrie, G. Zoumpoulidou, R.H. Te Poele, G.W. Aherne, S.C.
578 Wilson, P. Sheldrake, E. McDonald, M. Venet, C. Soudy, F. Elustondo, L. Rigoreau, J. Blagg,
579 P. Workman, M.D. Garrett, S. Mittnacht, Mechanism-based screen for G1/S checkpoint
580 activators identifies a selective activator of EIF2AK3/PERK signalling, PLoS One, 7 (2012)
581 e28568.
582 [19] N.A.S. Oliveira, B.R. Pinho, J. Pinto, P. Guedes de Pinho, J.M.A. Oliveira, Edaravone
583 counteracts redox and metabolic disruptions in an emerging zebrafish model of sporadic ALS,
584 Free Radic Biol Med, 217 (2024) 126-140.
585 [20] J. Hoyberghs, C. Bars, M. Ayuso, C. Van Ginneken, K. Foubert, S. Van Cruchten, DMSO
586 Concentrations up to 1% are Safe to be Used in the Zebrafish Embryo Developmental Toxicity
587 Assay, Front Toxicol, 3 (2021) 804033.
588 [21] R.F.O. Silva, B.R. Pinho, M.M. Santos, J.M.A. Oliveira, Disruptions of circadian rhythms,
589 sleep, and stress responses in zebrafish: New infrared-based activity monitoring assays for
590 toxicity assessment, Chemosphere, 305 (2022) 135449.
591 [22] B.R. Pinho, S.D. Reis, R.C. Hartley, M.P. Murphy, J.M.A. Oliveira, Mitochondrial
592 superoxide generation induces a parkinsonian phenotype in zebrafish and huntingtin
593 aggregation in human cells, Free Radic Biol Med, 130 (2019) 318-327.
594 [23] OECD, Test No. 236: Fish Embryo Acute Toxicity (FET) Test, (2013).

595 [24] C.B. Kimmel, W.W. Ballard, S.R. Kimmel, B. Ullmann, T.F. Schilling, Stages of
596 embryonic development of the zebrafish, Dev Dyn, 203 (1995) 253-310.
597 [25] R. Martinez, L. Navarro-Martin, C. Luccarelli, A.E. Codina, D. Raldua, C. Barata, R.
598 Tauler, B. Pina, Unravelling the mechanisms of PFOS toxicity by combining morphological
599 and transcriptomic analyses in zebrafish embryos, Sci Total Environ, 674 (2019) 462-471.
600 [26] B.R. Pinho, M.M. Santos, A. Fonseca-Silva, P. Valentao, P.B. Andrade, J.M. Oliveira,
601 How mitochondrial dysfunction affects zebrafish development and cardiovascular function: an
602 in vivo model for testing mitochondria-targeted drugs, Br J Pharmacol, 169 (2013) 1072-1090.
603 [27] N.A.S. Oliveira, B.R. Pinho, J.M.A. Oliveira, Swimming against ALS: How to model
604 disease in zebrafish for pathophysiological and behavioral studies, Neurosci Biobehav Rev,
605 148 (2023) 105138.
606 [28] B.R. Pinho, S.D. Reis, P. Guedes-Dias, A. Leitao-Rocha, C. Quintas, P. Valentao, P.B.
607 Andrade, M.M. Santos, J.M. Oliveira, Pharmacological modulation of HDAC1 and HDAC6 in
608 vivo in a zebrafish model: Therapeutic implications for Parkinson's disease, Pharmacol Res,
609 103 (2016) 328-339.
610 [29] J. Lee, D.W. Jung, W.H. Kim, J.I. Um, S.H. Yim, W.K. Oh, D.R. Williams, Development
611 of a highly visual, simple, and rapid test for the discovery of novel insulin mimetics in living
612 vertebrates, ACS Chem Biol, 8 (2013) 1803-1814.
613 [30] L. Wang, H. Kong, M. Jin, X. Li, R. Stoika, H. Lin, K. Liu, Synthesis of disaccharide
614 modified berberine derivatives and their anti-diabetic investigation in zebrafish using a
615 fluorescence-based technology, Org Biomol Chem, 18 (2020) 3563-3574.
616 [31] D. Stengel, F. Zindler, T. Braunbeck, An optimized method to assess ototoxic effects in
617 the lateral line of zebrafish (Danio rerio) embryos, Comp Biochem Physiol C Toxicol
618 Pharmacol, 193 (2017) 18-29.

619 [32] N. Tiso, E. Moro, F. Argenton, Zebrafish pancreas development, Mol Cell Endocrinol,
620 312 (2009) 24-30.
621 [33] R. Li, Y. Shen, An old method facing a new challenge: re-visiting housekeeping proteins
622 as internal reference control for neuroscience research, Life Sci, 92 (2013) 747-751.
623 [34] J. Jumper, R. Evans, A. Pritzel, T. Green, M. Figurnov, O. Ronneberger, K.
624 Tunyasuvunakool, R. Bates, A. Zidek, A. Potapenko, A. Bridgland, C. Meyer, S.A.A. Kohl,
625 A.J. Ballard, A. Cowie, B. Romera-Paredes, S. Nikolov, R. Jain, J. Adler, T. Back, S. Petersen,
626 D. Reiman, E. Clancy, M. Zielinski, M. Steinegger, M. Pacholska, T. Berghammer, S.
627 Bodenstein, D. Silver, O. Vinyals, A.W. Senior, K. Kavukcuoglu, P. Kohli, D. Hassabis,
628 Highly accurate protein structure prediction with AlphaFold, Nature, 596 (2021) 583-589.
629 [35] M. Varadi, S. Anyango, M. Deshpande, S. Nair, C. Natassia, G. Yordanova, D. Yuan, O.
630 Stroe, G. Wood, A. Laydon, A. Zidek, T. Green, K. Tunyasuvunakool, S. Petersen, J. Jumper,
631 E. Clancy, R. Green, A. Vora, M. Lutfi, M. Figurnov, A. Cowie, N. Hobbs, P. Kohli, G.
632 Kleywegt, E. Birney, D. Hassabis, S. Velankar, AlphaFold Protein Structure Database:
633 massively expanding the structural coverage of protein-sequence space with high-accuracy
634 models, Nucleic Acids Res, 50 (2022) D439-D444.
635 [36] J.M. Axten, J.R. Medina, Y. Feng, A. Shu, S.P. Romeril, S.W. Grant, W.H. Li, D.A.
636 Heerding, E. Minthorn, T. Mencken, C. Atkins, Q. Liu, S. Rabindran, R. Kumar, X. Hong, A.
637 Goetz, T. Stanley, J.D. Taylor, S.D. Sigethy, G.H. Tomberlin, A.M. Hassell, K.M. Kahler,
638 L.M. Shewchuk, R.T. Gampe, Discovery of 7-methyl-5-(1-{[3-
639 (trifluoromethyl)phenyl]acetyl}-2,3-dihydro-1H-indol-5-yl)-7H-p yrrolo[2,3-d]pyrimidin-4-
640 amine (GSK2606414), a potent and selective first-in-class inhibitor of protein kinase R (PKR)-
641 like endoplasmic reticulum kinase (PERK), J Med Chem, 55 (2012) 7193-7207.

642 [37] C. Chintha, A. Carlesso, A.M. Gorman, A. Samali, L.A. Eriksson, Molecular modeling
643 provides a structural basis for PERK inhibitor selectivity towards RIPK1, RSC Adv, 10 (2019)
644 367-375.
645 [38] O. Carugo, S. Pongor, A normalized root-mean-square distance for comparing protein
646 three-dimensional structures, Protein Sci, 10 (2001) 1470-1473.
647 [39] M.M. Rahman, T. Basta, J. Teng, M. Lee, B.T. Worrell, M.H.B. Stowell, R.E. Hibbs,
648 Structural mechanism of muscle nicotinic receptor desensitization and block by curare, Nat
649 Struct Mol Biol, 29 (2022) 386-394.
650 [40] L. Guzman, G. Besa, D. Linares, L. González, C. Pont, M. Bartolini, A. Haigis, J. Legradi,
651 D. Muñoz-Torrero, J. Gómez-Catalán, M. Barenys, Evaluation of the effects of
652 acetylcholinesterase inhibitors in the zebrafish touch-evoked response: quantitative vs.
653 qualitative assessment, Environ Sci Eur, 32 (2020) 12.
654 [41] A. Sumegi, Z. Hendrik, T. Gall, E. Felszeghy, K. Szakszon, P. Antal-Szalmas, L. Beke,
655 A. Papp, G. Mehes, J. Balla, G. Balla, A novel splice site indel alteration in the EIF2AK3 gene
656 is responsible for the first cases of Wolcott-Rallison syndrome in Hungary, BMC Med Genet,
657 21 (2020) 61.
658 [42] O. Rubio-Cabezas, A.M. Patch, J.A. Minton, S.E. Flanagan, E.L. Edghill, K. Hussain, A.
659 Balafrej, A. Deeb, C.R. Buchanan, I.G. Jefferson, A. Mutair, G. Neonatal Diabetes
660 International Collaborative, A.T. Hattersley, S. Ellard, Wolcott-Rallison syndrome is the most
661 common genetic cause of permanent neonatal diabetes in consanguineous families, J Clin
662 Endocrinol Metab, 94 (2009) 4162-4170.
663 [43] K. Iida, Y. Li, B.C. McGrath, A. Frank, D.R. Cavener, PERK eIF2 alpha kinase is required
664 to regulate the viability of the exocrine pancreas in mice, BMC Cell Biol, 8 (2007) 38.
665 [44] D. Aldrian, C. Bochdansky, A.M. Kavallar, C. Mayerhofer, A. Deeb, A. Habeb, A.
666 Romera Rabasa, A. Khadilkar, A. Ucar, B. Knoppke, D. Zafeiriou, M. Lang-Muritano, M.

667 Miqdady, S. Judmaier, V. McLin, V. Furdela, T. Muller, G.F. Vogel, Natural history of
668 Wolcott-Rallison syndrome: A systematic review and follow-up study, Liver Int, 44 (2024)
669 811-822.
670 [45] M.C. de Wit, I.F. de Coo, C. Julier, M. Delepine, M.H. Lequin, I. van de Laar, B.J. Sibbles,
671 G.J. Bruining, G.M. Mancini, Microcephaly and simplified gyral pattern of the brain associated
672 with early onset insulin-dependent diabetes mellitus, Neurogenetics, 7 (2006) 259-263.
673 [46] Y. Abdelmeguid, E.W. Mowafy, I. Marzouk, E. Franco, S. ElSayed, Clinical and
674 molecular characteristics of infantile-onset diabetes mellitus in Egypt, Ann Pediatr Endocrinol
675 Metab, 27 (2022) 214-222.
676 [47] C.M. Thornton, D.J. Carson, F.J. Stewart, Autopsy findings in the Wolcott-Rallison
677 syndrome, Pediatr Pathol Lab Med, 17 (1997) 487-496.
678 [48] R. Bejiqi, R. Retkoceri, N. Zeka, R. Bejiqi, S. Bejic, An Infant With Neonatal Diabetes
679 and Double Outlet Right Ventricle - Wolcott- Rallison syndrome, Med Arch, 72 (2018) 289-
680 291.
681 [49] F. Zindler, F. Beedgen, D. Brandt, M. Steiner, D. Stengel, L. Baumann, T. Braunbeck,
682 Analysis of tail coiling activity of zebrafish (Danio rerio) embryos allows for the differentiation
683 of neurotoxicants with different modes of action, Ecotoxicol Environ Saf, 186 (2019) 109754.
684 [50] A.C. Roberts, J. Chornak, J.B. Alzagatiti, D.T. Ly, B.R. Bill, J. Trinkeller, K.C. Pearce,
685 R.C. Choe, C.S. Campbell, D. Wong, E. Deutsch, S. Hernandez, D.L. Glanzman, Rapid
686 habituation of a touch-induced escape response in Zebrafish (Danio rerio) Larvae, PLoS One,
687 14 (2019) e0214374.
688 [51] M. von Wyl, S. Konemann, C. Vom Berg, Different developmental insecticide exposure
689 windows trigger distinct locomotor phenotypes in the early life stages of zebrafish,
690 Chemosphere, 317 (2023) 137874.

691 [52] J. Berger, T. Sztal, P.D. Currie, Quantification of birefringence readily measures the level
692 of muscle damage in zebrafish, Biochem Biophys Res Commun, 423 (2012) 785-788.
693 [53] J.A. Moreno, M. Halliday, C. Molloy, H. Radford, N. Verity, J.M. Axten, C.A. Ortori,
694 A.E. Willis, P.M. Fischer, D.A. Barrett, G.R. Mallucci, Oral treatment targeting the unfolded
695 protein response prevents neurodegeneration and clinical disease in prion-infected mice, Sci
696 Transl Med, 5 (2013) 206ra138.
697 [54] R. Cagnetta, H.H. Wong, C.K. Frese, G.R. Mallucci, J. Krijgsveld, C.E. Holt,
698 Noncanonical Modulation of the eIF2 Pathway Controls an Increase in Local Translation
699 during Neural Wiring, Mol Cell, 73 (2019) 474-489 e475.
700 [55] D. Rojas-Rivera, T. Delvaeye, R. Roelandt, W. Nerinckx, K. Augustyns, P. Vandenabeele,
701 M.J.M. Bertrand, When PERK inhibitors turn out to be new potent RIPK1 inhibitors: critical
702 issues on the specificity and use of GSK2606414 and GSK2656157, Cell Death Differ, 24
703 (2017) 1100-1110.
704 [56] M. Mahameed, T. Wilhelm, O. Darawshi, A. Obiedat, W.S. Tommy, C. Chintha, T.
705 Schubert, A. Samali, E. Chevet, L.A. Eriksson, M. Huber, B. Tirosh, The unfolded protein
706 response modulators GSK2606414 and KIRA6 are potent KIT inhibitors, Cell Death Dis, 10
707 (2019) 300.
708 [57] W. Wen, J. Chen, Y. Zhou, G. Li, Y. Zhang, Loss of Ripk3 attenuated neutrophil
709 accumulation in a lipopolysaccharide-induced zebrafish inflammatory model, Cell Death
710 Discov, 8 (2022) 88.
711 [58] K.A. Hultman, N. Bahary, L.I. Zon, S.L. Johnson, Gene Duplication of the zebrafish kit
712 ligand and partitioning of melanocyte development functions to kit ligand a, PLoS Genet, 3
713 (2007) e17.
714 [59] Y. Li, K. Iida, J. O'Neil, P. Zhang, S. Li, A. Frank, A. Gabai, F. Zambito, S.H. Liang, C.J.
715 Rosen, D.R. Cavener, PERK eIF2alpha kinase regulates neonatal growth by controlling the

716 expression of circulating insulin-like growth factor-I derived from the liver, Endocrinology,
717 144 (2003) 3505-3513.
718 [60] J. Wei, X. Sheng, D. Feng, B. McGrath, D.R. Cavener, PERK is essential for neonatal
719 skeletal development to regulate osteoblast proliferation and differentiation, J Cell Physiol, 217
720 (2008) 693-707.
721 [61] F. Tonelli, J.W. Bek, R. Besio, A. De Clercq, L. Leoni, P. Salmon, P.J. Coucke, A.
722 Willaert, A. Forlino, Zebrafish: A Resourceful Vertebrate Model to Investigate Skeletal
723 Disorders, Front Endocrinol (Lausanne), 11 (2020) 489.
724 [62] D.R. Cavener, S. Gupta, B.C. McGrath, PERK in beta cell biology and insulin biogenesis,
725 Trends Endocrinol Metab, 21 (2010) 714-721.
726 [63] A. Welters, T. Meissner, K. Konrad, C. Freiberg, K. Warncke, S. Judmaier, O.
727 Kordonouri, M. Wurm, M. Papsch, G. Fitzke, S.C. Schmidt, S.R. Tittel, R.W. Holl, Diabetes
728 management in Wolcott-Rallison syndrome: analysis from the German/Austrian DPV
729 database, Orphanet J Rare Dis, 15 (2020) 100.
730 [64] D. Feng, J. Wei, S. Gupta, B.C. McGrath, D.R. Cavener, Acute ablation of PERK results
731 in ER dysfunctions followed by reduced insulin secretion and cell proliferation, BMC Cell
732 Biol, 10 (2009) 61.
733 [65] W. Zhang, D. Feng, Y. Li, K. Iida, B. McGrath, D.R. Cavener, PERK EIF2AK3 control
734 of pancreatic beta cell differentiation and proliferation is required for postnatal glucose
735 homeostasis, Cell Metab, 4 (2006) 491-497.
736 [66] C.R. Sowers, R. Wang, R.A. Bourne, B.C. McGrath, J. Hu, S.C. Bevilacqua, J.C. Paton,
737 A.W. Paton, S. Collardeau-Frachon, M. Nicolino, D.R. Cavener, The protein kinase
738 PERK/EIF2AK3 regulates proinsulin processing not via protein synthesis but by controlling
739 endoplasmic reticulum chaperones, J Biol Chem, 293 (2018) 5134-5149.

740 [67] L. Zang, L.A. Maddison, W. Chen, Zebrafish as a Model for Obesity and Diabetes, Front
741 Cell Dev Biol, 6 (2018) 91.
742 [68] J.B. Moss, P. Koustubhan, M. Greenman, M.J. Parsons, I. Walter, L.G. Moss,
743 Regeneration of the pancreas in adult zebrafish, Diabetes, 58 (2009) 1844-1851.
744 [69] H. Pisharath, J.M. Rhee, M.A. Swanson, S.D. Leach, M.J. Parsons, Targeted ablation of
745 beta cells in the embryonic zebrafish pancreas using E. coli nitroreductase, Mech Dev, 124
746 (2007) 218-229.
747 [70] C. Karampelias, K.C. Liu, A. Tengholm, O. Andersson, Mechanistic insights and
748 approaches for beta cell regeneration, Nat Chem Biol, (2025).
749 [71] S.N. Asl, R. Vakili, S. Vakili, F. Soheilipour, M. Hashemipour, S. Ghahramani, E. De
750 Franco, H. Yaghootkar, Wolcott-Rallison syndrome in Iran: a common cause of neonatal
751 diabetes, J Pediatr Endocrinol Metab, 32 (2019) 607-613.
752 [72] F. Longo, M. Mancini, P.L. Ibraheem, S. Aryal, C. Mesini, J.C. Patel, E. Penhos, N.
753 Rahman, M. Mamcarz, E. Santini, M.E. Rice, E. Klann, Cell-type-specific disruption of PERK-
754 eIF2alpha signaling in dopaminergic neurons alters motor and cognitive function, Mol
755 Psychiatry, 26 (2021) 6427-6450.
756 [73] D. Bournele, D. Beis, Zebrafish models of cardiovascular disease, Heart Fail Rev, 21
757 (2016) 803-813.
758 [74] K.M. Ross Stewart, S.L. Walker, A.H. Baker, P.R. Riley, M. Brittan, Hooked on heart
759 regeneration: the zebrafish guide to recovery, Cardiovasc Res, 118 (2022) 1667-1679.
760 [75] C. Cornet, V. Di Donato, J. Terriente, Combining Zebrafish and CRISPR/Cas9: Toward
761 a More Efficient Drug Discovery Pipeline, Front Pharmacol, 9 (2018) 703.
762

Figures

A Global amino acid comparison

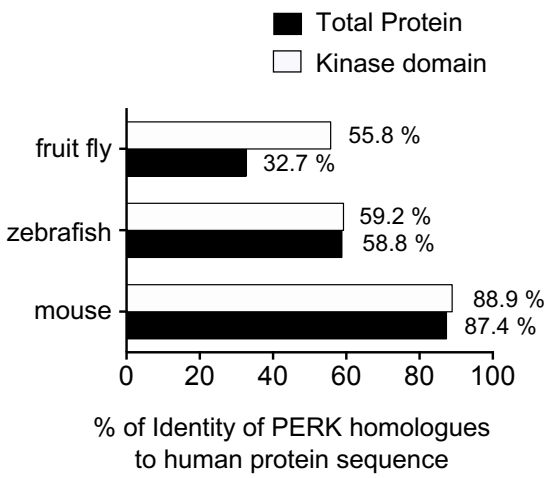

B Comparison of vital* amino acids in kinase domain

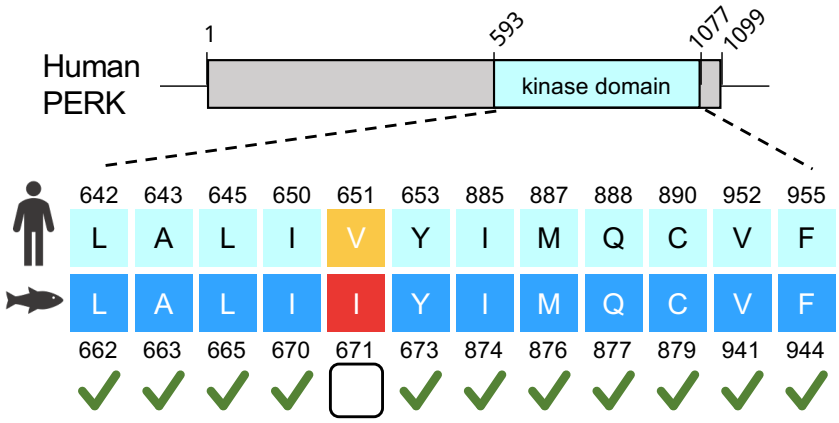

* 12 vital amino acids for GSK2606414 binding

valine (V) and isoleucine (I) are both hydrophobic

C Molecular visualization of GSK binding to PERK

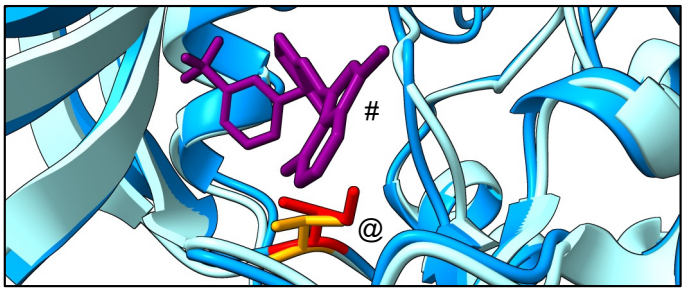

human PERK

zebrafish PERK

@, valine 651 (human)

@, isoleucine 671 (zebrafish)

#, GSK2606414 (GSK)

D Structural similarity of human vs. zebrafish PERK

Root Mean Square Deviation		
Total protein	0.868 Å	**High similarity** (0-1 Å)
Catalytic domain	0.371 Å	**High similarity** (0-1 Å)

Figure 1

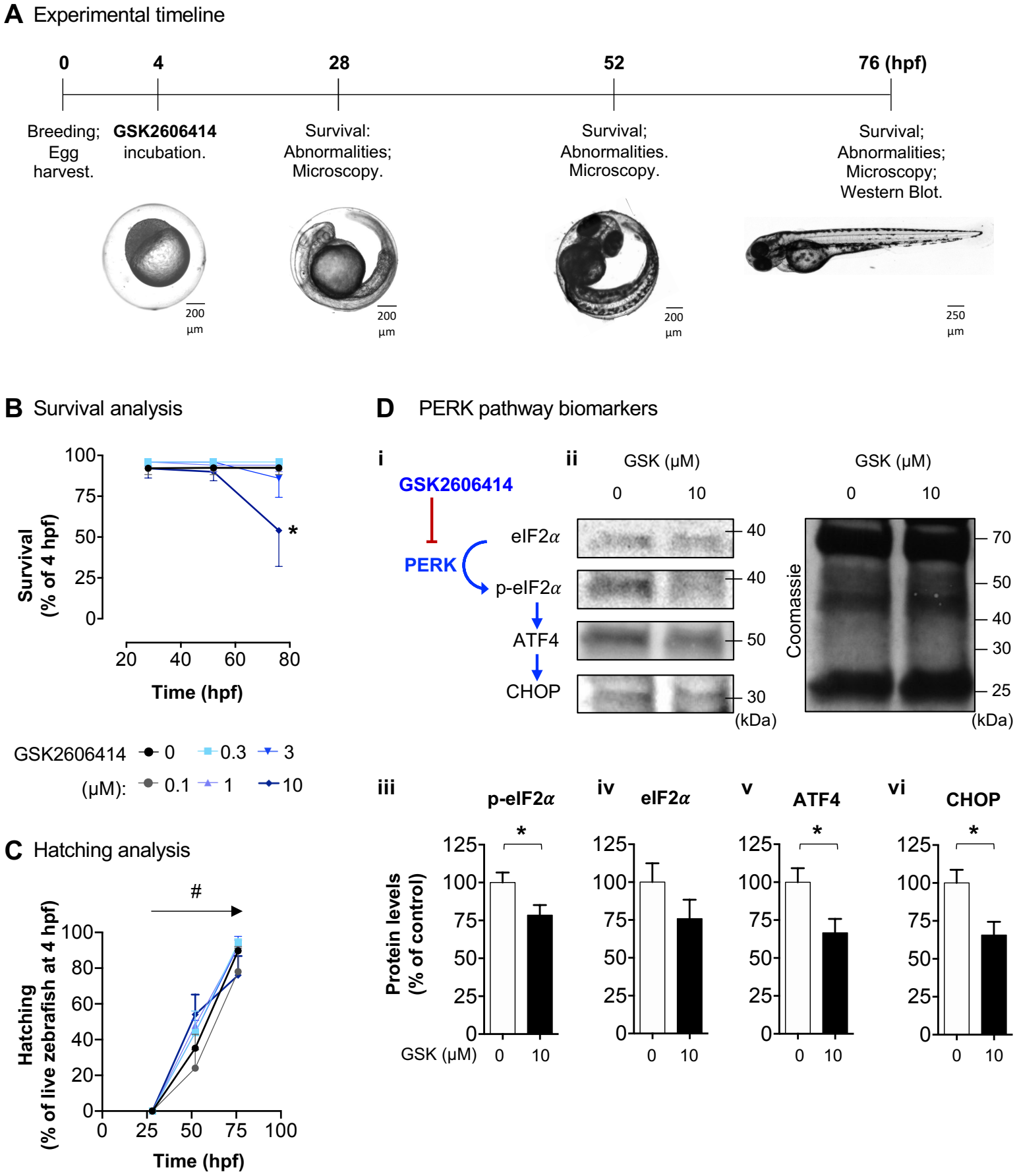
A Experimental timeline
0
4
28
52
76 (hpf)
Breeding; Egg harvest.
GSK2606414 incubation.
Survival: Abnormalities; Microscopy.
Survival; Abnormalities. Microscopy.
Survival; Abnormalities; Microscopy; Western Blot.
200 µm
200 µm
200 µm
250 µm
B Survival analysis
Survival (% of 4 hpf)
Time (hpf)
GSK2606414 (µM): 0 0.3 3 0.1 1 10
C Hatching analysis
Hatching (% of live zebrafish at 4 hpf)
Time (hpf)
D PERK pathway biomarkers
i
GSK2606414
PERK
eIF2α
p-eIF2α
ATF4
CHOP
ii
GSK (µM)
0 10
(kDa)
Coomassie
iii p-eIF2α
iv eIF2α
v ATF4
vi CHOP
Protein levels (% of control)
GSK (µM) 0 10

Figure 2

A Morphological defects

i

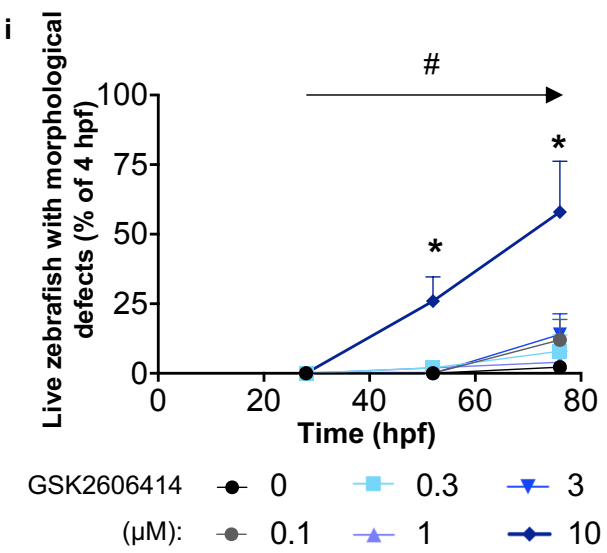

ii

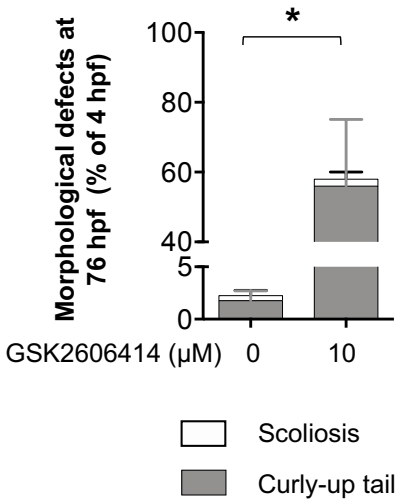

iii – Normal morphology

iv – Curly-up tail

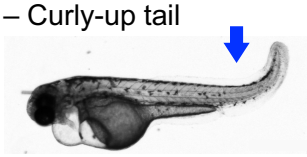

v – Scoliosis

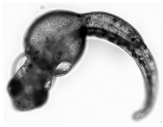

500 μm

B Trunk-tail angle

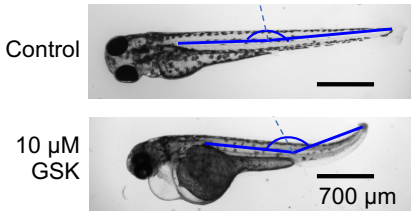

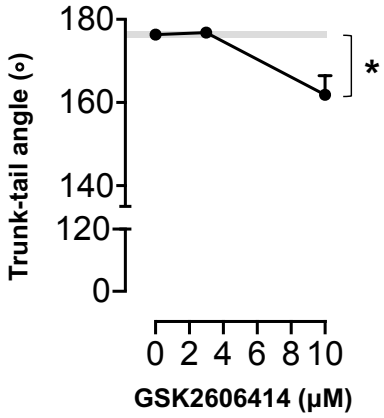

C Body length

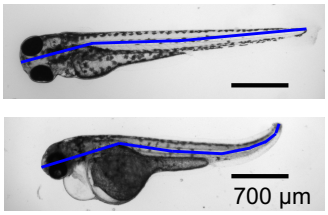

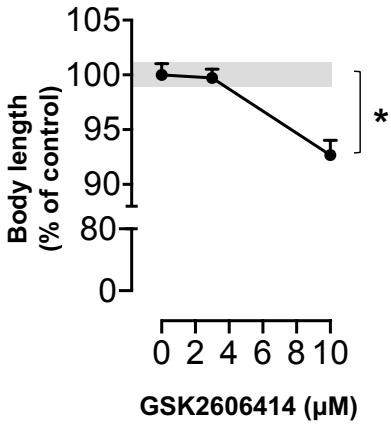

D **Positive control for tubocurarine (dTC)**

i – Head reflex

ii – Tail reflex

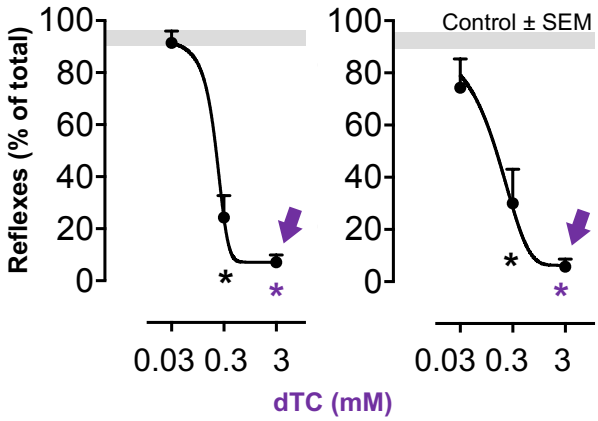

E **The muscle relaxant tubocurarine (dTC) does not rescue the curly-up tail evoked by GSK2606414**

i – Control

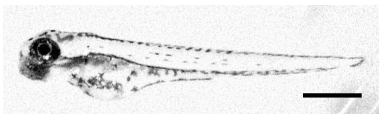

ii – 3 mM dTC

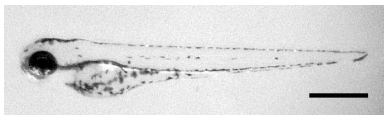

iii – 10 μM GSK2606414

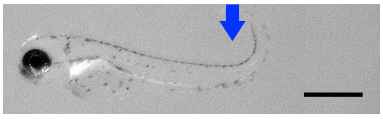

iv - 10 μM GSK2606414 + 3 mM dTC

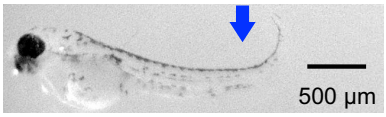

v

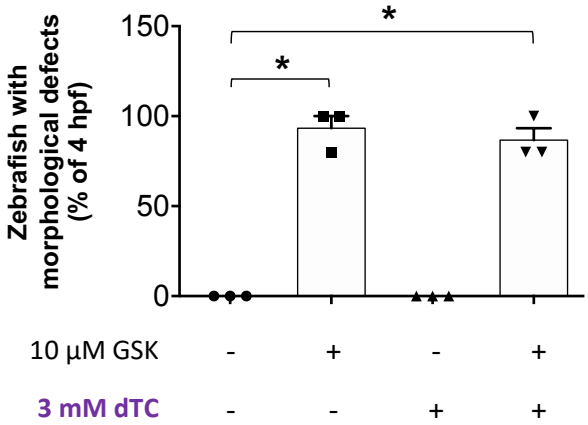

Figure 3

Figure 4

A Pancreatic development

i 28 hpf

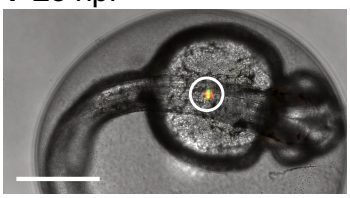

ins:GFP + sst:mCherry

ii 76 hpf

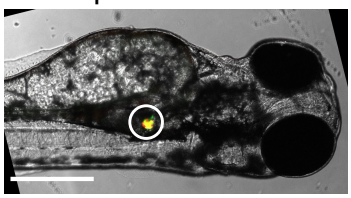

ins:GFP + sst:mCherry

iii 148 hpf

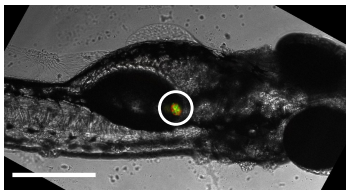

ins:GFP+ sst:mCherry

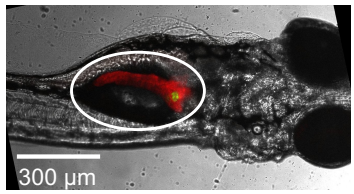

ins:GFP + ela:mCherry

B

i Early (4 hpf) GSK exposure protocol

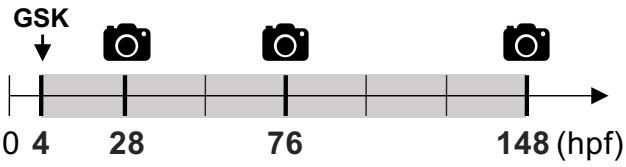

ii Late (76 hpf) GSK exposure protocol

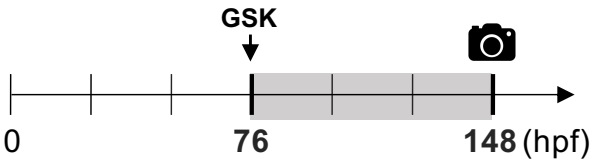

C *ins:GFP* (*β* cell; endocrine)

i Early: 4 hpf → 28 hpf 76 hpf 148 hpf

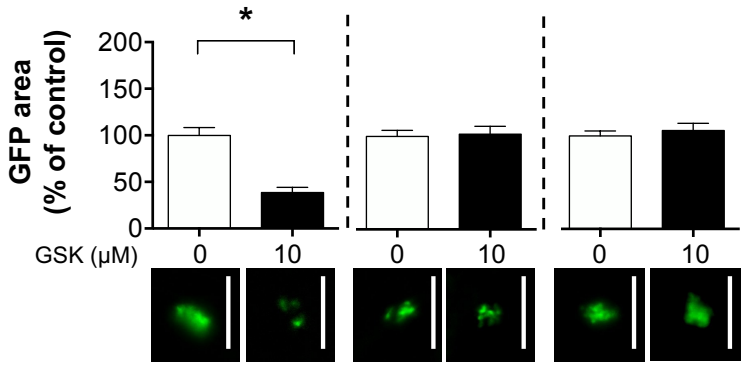

ii Late: 76 hpf → 148 hpf

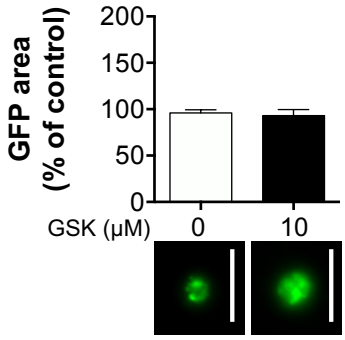

D *sst:mCherry* (*δ* cell; endocrine)

i Early: 4 hpf → 28 hpf 76 hpf 148 hpf

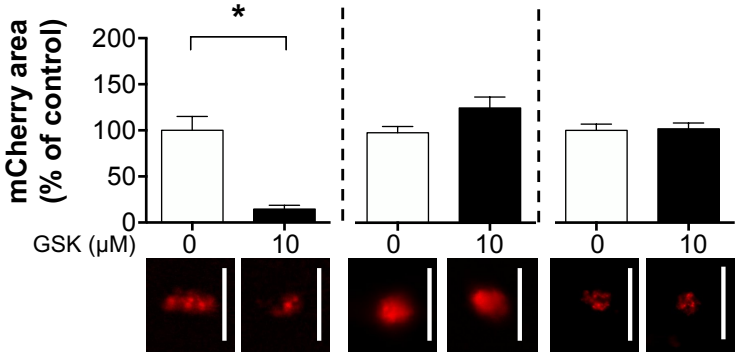

ii Late: 76 hpf → 148 hpf

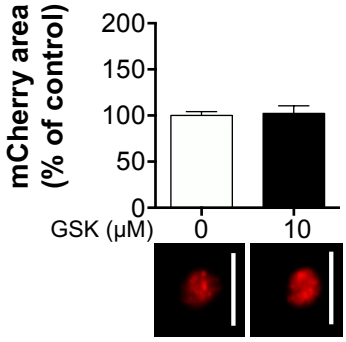

E *ela:mCherry* (exocrine)

i Early: 4 hpf → 148 hpf

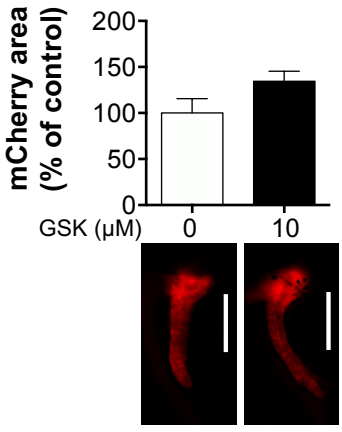

ii Late: 76 hpf → 148 hpf

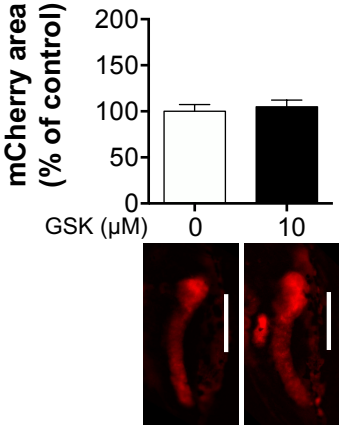

A 2-NBD glucose uptake to neuromasts

i Control

ii 10 μM GSK2606414

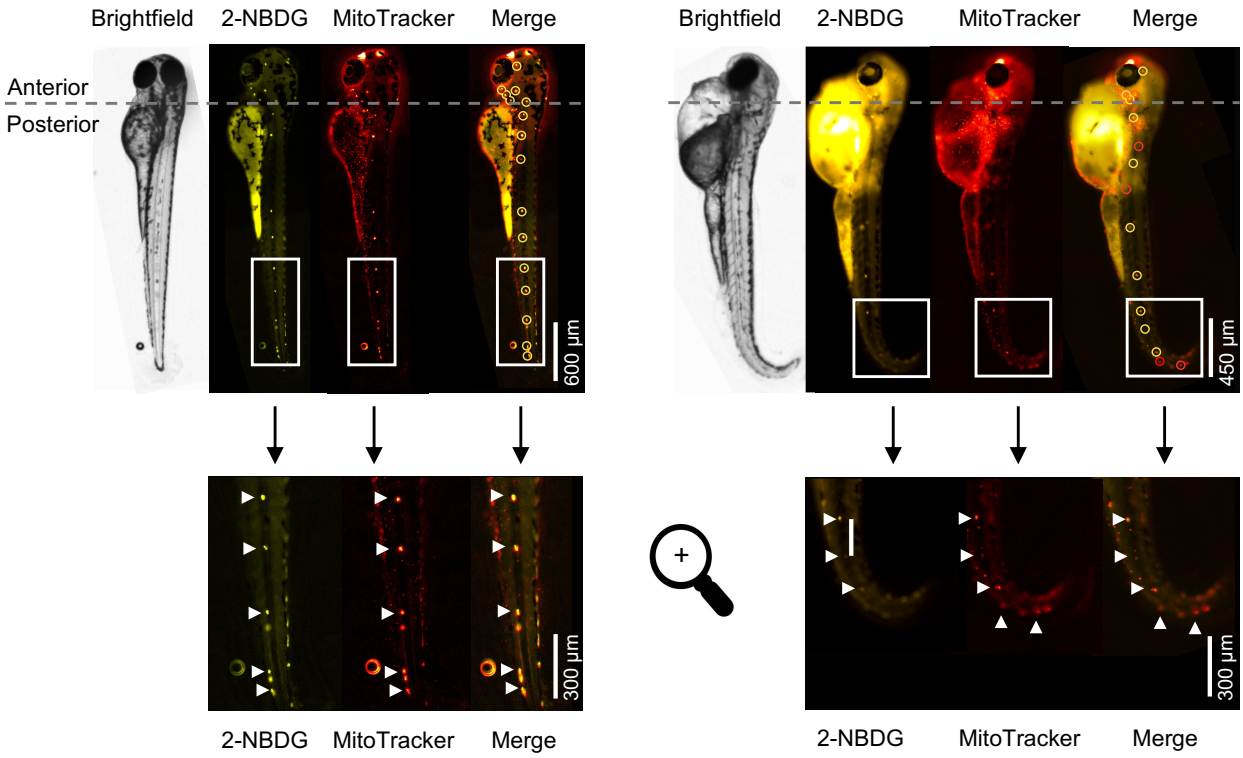

B Neuromast quantification

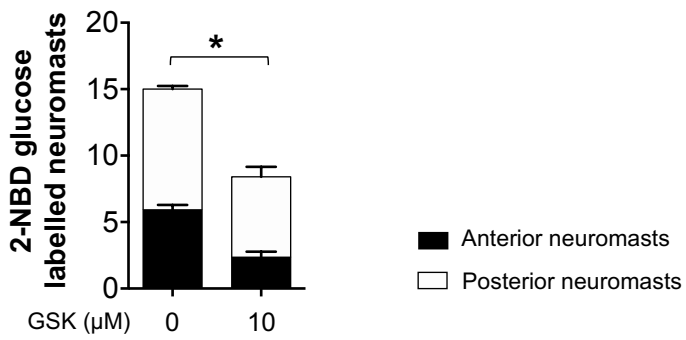

Figure 5

A Tail coiling events (28 hpf)

i

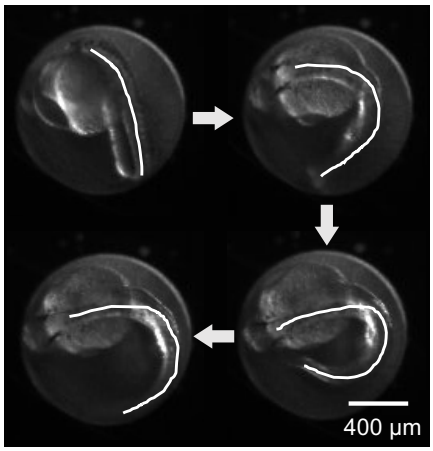

ii

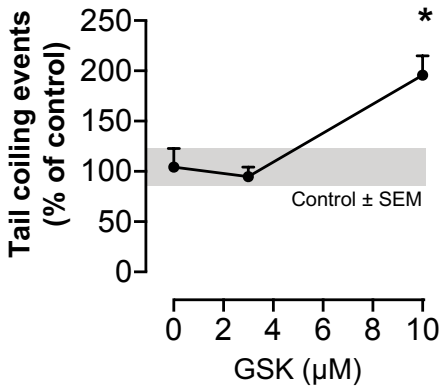

B Touch-evoked escape responses (76 hpf)

i

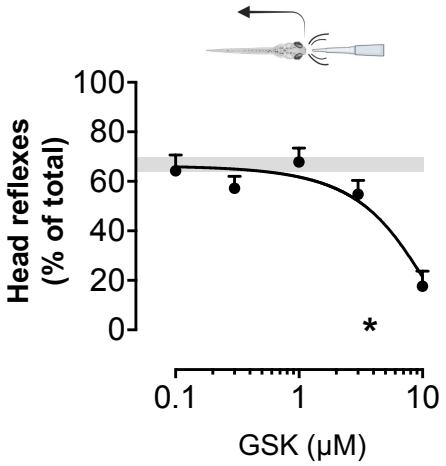

ii

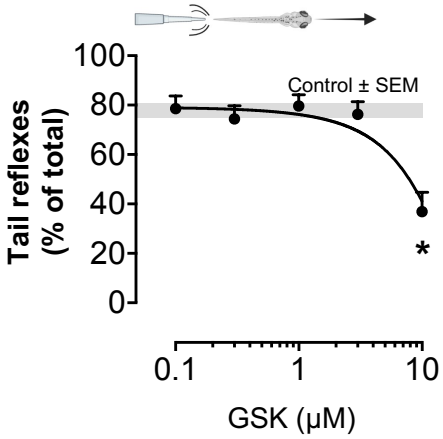

C Birefringence assay (76 hpf)

i

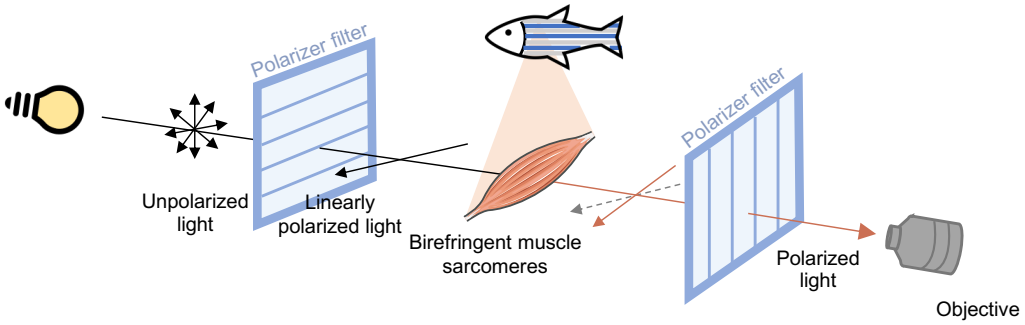

ii

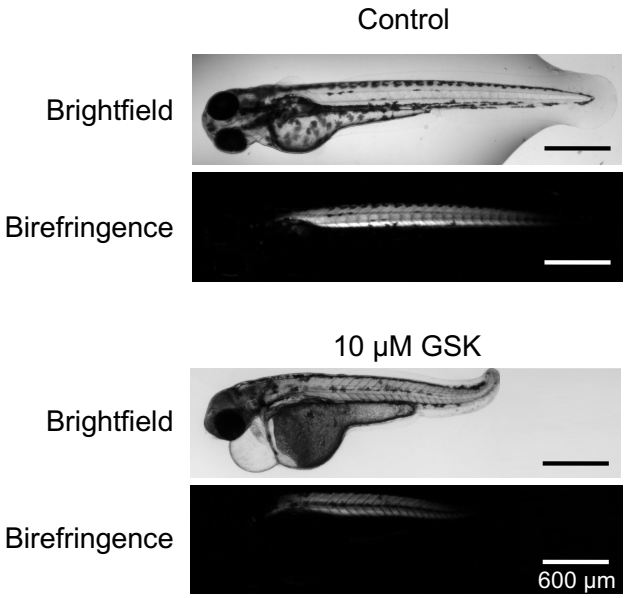

iii

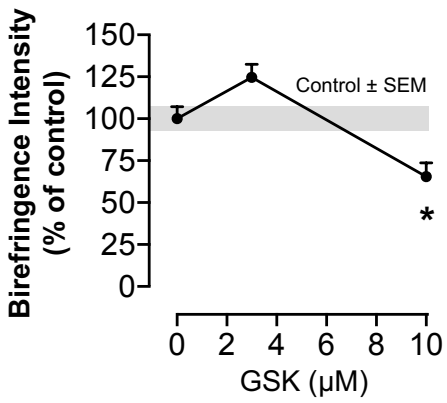

Figure 6

A Pericardial oedema

i

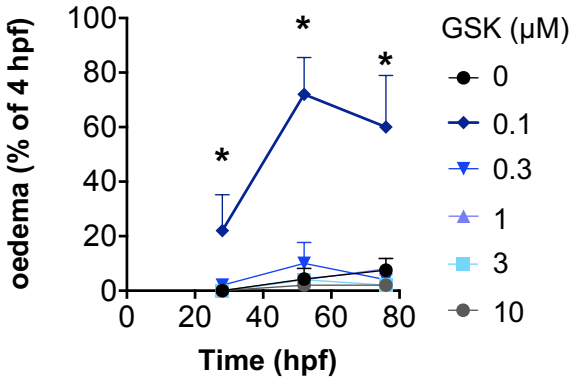

ii 28 hpf **iii** 76 hpf

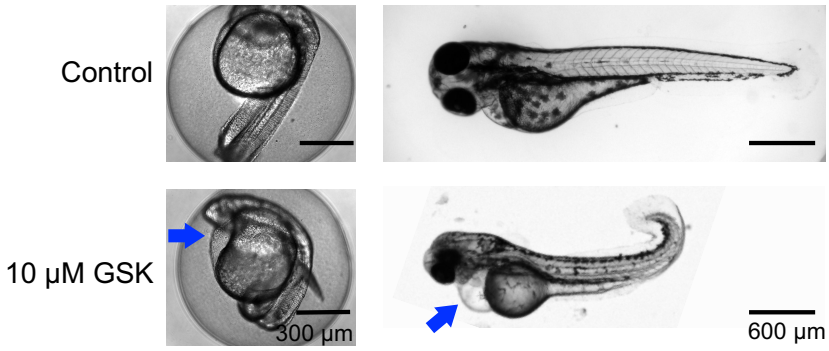

B Heart beat analysis

i

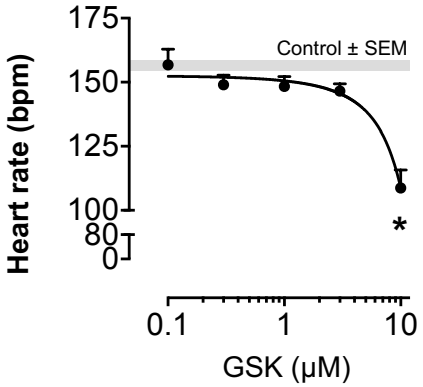

ii

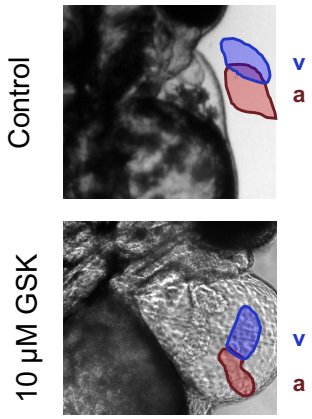

Atrio-ventricular coordination

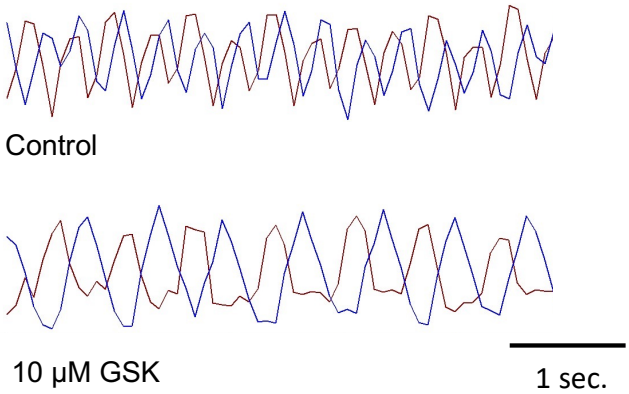

Figure 7

Supplementary Material

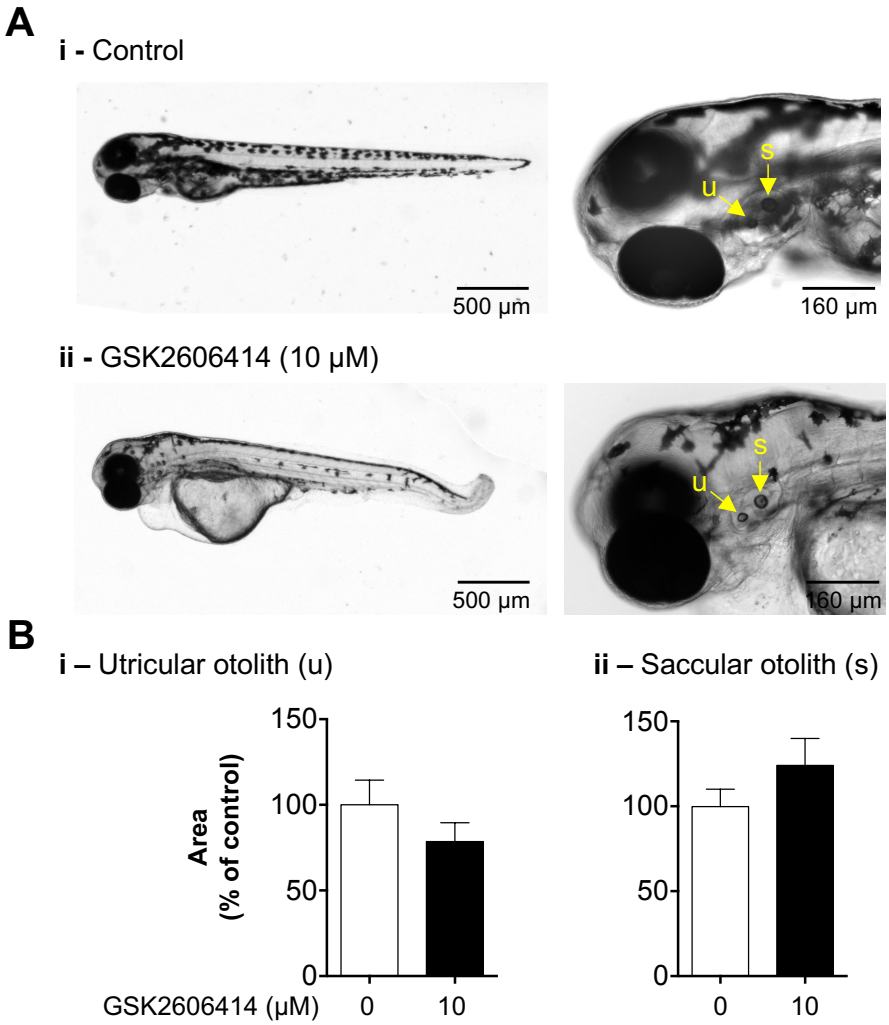

Supplementary Figure 1. GSK2606414 (GSK) does not alter zebrafish otolith area. **(A)** Representative images of zebrafish at 76hpf following treatment with control (0 µM GSK) or 10 µM GSK since 4 hpf. Arrows: (u) utricular/anterior otolith, (s) saccular/posterior otolith. **(B)** Mean ± SEM of the otolith area, $P > 0.05$, t-test, $n = 15$ larvae, 3 zebrafish experiments.

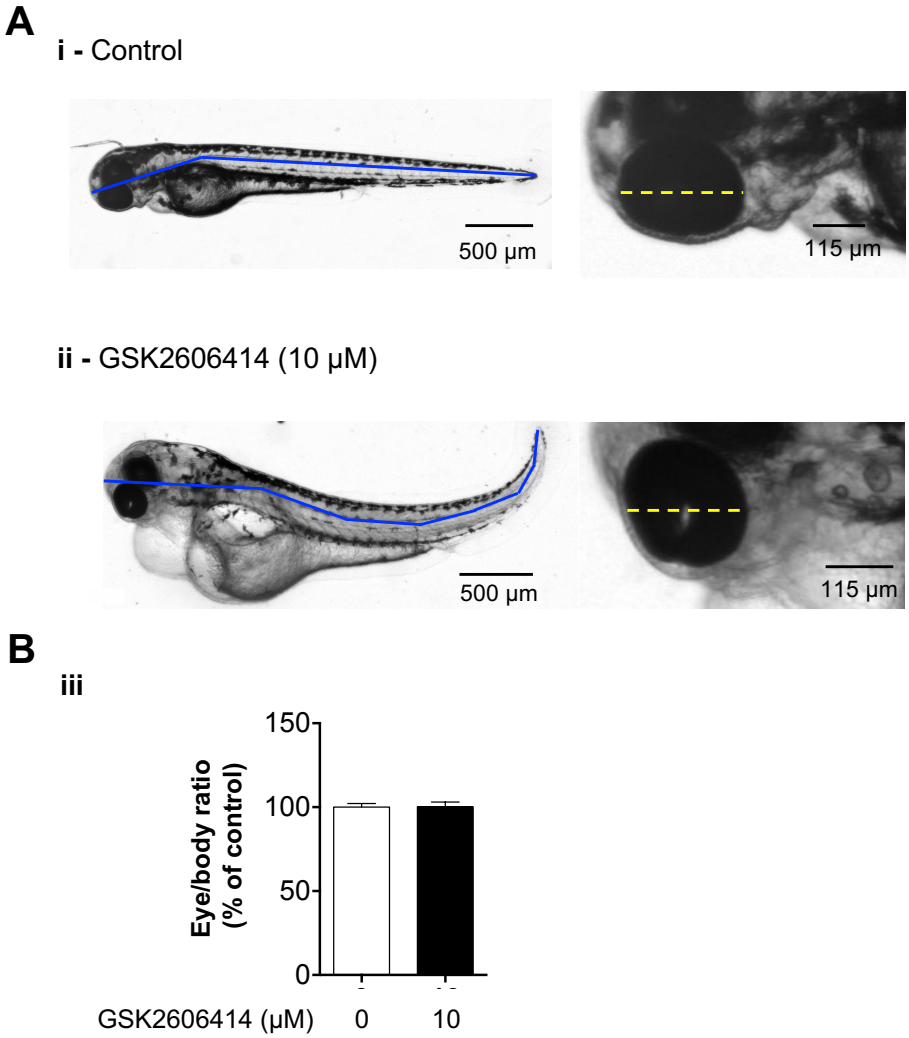

Supplementary Figure 2. GSK2606414 does not alter zebrafish eye/body ratio. **(A)** Representative images of zebrafish at 76hpf following treatment with control (0 µM GSK) or 10 µM GSK since 4 hpf. Solid blue lines: body length; dashed yellow lines: eye diameter. **(B)** Mean ± SEM of the eye/body ratio, $P > 0.05$, t-test, $n = 15$ zebrafish, 3 independent experiments.

Supplementary Table 1. Primary antibodies used in western blots from Fig. 2 D.

Antibody	Dilution	Supplier	Catalog Number	RRID
anti-ATF4	1:500	Proteintech	Cat# 10835-1-AP	AB_2058600
anti-CHOP	1:1000	Proteintech	Cat# 15204-1-AP	AB_2292610
anti-eIF2α	1:1000	Thermo Fisher Scientific	Cat# AHO0802	AB_2536316
anti-p-eIF2α	1:500	Thermo Fisher Scientific	Cat# MA5-15133	AB_10983400

Supplementary Table 2. Secondary antibodies used in western blots from Fig. 2 D.

Antibody	Dilution	Supplier	Catalog Number	RRID
anti-mouse	1:4000	Thermo Fisher Scientific	Cat# G-21040	AB_2536527
anti-rabbit	1:4000	Thermo Fisher Scientific	Cat# G-21234	AB_2536530